The Individualistic Dynamics of Entangled DNA in Solution

Rodrigo E. Teixeira,[||] Ajey K. Dambal,[†] David H. Richter,[‡] Eric S. G. Shaqfeh,*[,†,‡] and Steven Chu[§]

Department of Chemical Engineering, Stanford University, Stanford, California 94305, Department of Mechanical Engineering, Stanford University, Stanford, California 94305, Lawrence Berkeley National Laboratory, Berkeley, California 94720

Received December 21, 2006

ABSTRACT: We present the direct visualizations of single, entangled DNA polymers in three flow experiments: relaxation following a rapid shear deformation, steady shear, and startup shear. To evaluate molecular theories, "test" chains were stained against a background of unstained but otherwise identical chains. To provide a direct link to bulk viscoelasticity, identical preparations were also extensively characterized via mechanical rheometry. The four concentrations studied displayed similar rheological features to synthetic polymers at comparable concentrations and were accordingly classified from semidilute to well-entangled. In entangled solutions, we uncovered two distinct relaxation time scales, with the fast, chain retraction characteristic time, $\tau_{fast} \approx 10$-fold longer than the rotational Rouse time assumed by theoretical models. We also found a high degree of molecular individualism and broad conformational distributions in all experiments at shear rates $\dot{\gamma} > \tau_{fast}^{-1}$. This new evidence restricts the applicability of the pre-averaging approximation underlying all closed-form theories developed to date and explains some of the complications in modeling nonlinear flows.

Introduction

Research activity and basic understanding in the flow behavior of linear entangled polymers has grown considerably in the last 30 years to become one of the most rapidly expanding fields of soft condensed matter physics. One of the earliest seminal ideas was Edward's introduction of the tube mean-field-like approximation.[1] He reasoned that the collective interactions between any given molecule under consideration, called the "test" chain, and its neighboring chains could be safely simplified as a confining "tube" potential following the contour of the test chain. The tube picture led DeGennes to propose the concept of *reptation*, or the idea that polymers could relax their conformation, and hence the stresses felt throughout the fluid, as they diffused along their own contour to sample more random orientations.[2] De Gennes also aptly predicted that the characteristic timescales for the test chain to disengage from its original tube, termed the disengagement time τ_d, should scale as the cube of the molecular weight. Borrowing from these conceptual breakthroughs, Doi and Edwards were the first to formulate the mechanism of reptation into convenient mathematical terms that made it possible to write a constitutive equation (stress−strain relation) based on molecular-level arguments.[3−7] A great success of the Doi−Edwards (DE) theory is the damping function in a step-shear strain experiment, a signature of nonlinear shear flow deformation. Until that time, no theory had been able to describe the nonlinear response of entangled systems.

Despite its great overall success, the DE theory failed to predict the correct steady shear stress. Instead of a plateau after the initial rise, The DE theory showed a decrease, which would imply a shear banding instability at moderately high shear rates. After many follow-up experiments, such an instability was not found. One simplifying assumption made in the DE theory was that chain retraction occurred instantaneously. In other words, no flow was strong enough to stretch a polymer beyond its original equilibrium primitive path length (the length of the confining tube under linear flows). For the chain to be able to stretch, a time scale for chain retraction had to be introduced. This modification was incorporated to the DE theory by Marrucci and Grizzuti, resulting in what is called the DEMG theory.[8−10] This modification led to a series of improved predictions. These included more accurate overshoots in shear stress and first normal stress difference. Nevertheless, the theory still failed to remove the local maximum in shear stress. Theorists conjectured that this and other failures were related to an excessive degree of chain orientation in shear flow. By then, all theories allowed the average conformation to reach a very close alignment with the flow, causing the frictional forces on the chain to be severely reduced, which results in an anomalous decay of viscosity.

In 1996, Marrucci introduced the concept of convective constraint release (CCR), which resolved the key problem with the DE and his DEMG theory.[11] Marrucci reasoned that, while reptation seemed to be the correct relaxation mechanism for fluids at rest or at slow flows, at some point in faster flows, chains must start to preferentially convect past each other instead of reptating. If two adjacent chains acquire a relative velocity between them, then any entanglements from the interaction of the two would be forgotten. By the same reasoning, two noninteracting chains could become entangled at a later time. In fact, any given chain would be subjected to a continuous annihilation and creation of entanglements, with the latter termed *tube renewal.* This process would allow each chain time to relax, thus preventing excessive alignment. By the same reasoning, the rate of tube renewal should then be proportional to the local velocity gradient (e.g., the shear rate in shear flows), so relaxation matches the rate of deformation, which gives rise, for instance, to the broad plateau in shear stress routinely observed in rheology measurements.

* To whom correspondence should be addressed. E-mail: esgs@stanford.com.
[†] Department of Chemical Engineering, Stanford University.
[‡] Department of Mechanical Engineering, Stanford University.
[§] Lawrence Berkeley National Laboratory.
[||] Present address: Department of Computational Medicine and Biology, CFD Research Corp., Huntsville, Alabama 35805.

10.1021/ma062932e CCC: $37.00
Published on Web 03/03/2007

Incorporating CCR into a new theory while retaining the correct features of the DEMG theory has proven difficult, however. Initial attempts by Marrucci himself acquired a much simplified form or used ad hoc variables.[12−14] More recently, Mead, Larson, and Doi have advanced a theory capable of reproducing, at least in qualitative fashion, all linear and some nonlinear bulk rheological characteristics.[15] Their description utilizes two coarse-grained molecular parameters: the *tube stretch* and *orientation*. While this theory reproduces some bulk rheological behavior, it fails to capture the extinction angle from birefringence experiments. To reproduce the extinction angle as well, the authors then proposed a finer-grained, *contour variable* version of their theory. This more sophisticated alternative utilizes the full test chain's conformation at the resolution of single entanglement strands or segments of polymer lying between two adjacent entanglement points. Using a different formalism approach, Graham and co-workers from McLeish's group[16−18] have also proposed a contour variable theory. Their theory is more general than the MLD theory because it bypasses the need for an *ad hoc* "switch function" between reptation and tube stretch. This theory demonstrated a broad range of excellent quantitative reproductions for the bulk response and good agreement with small-angle neutron scattering (SANS) data.[19−21]

With their high level of sophistication, current molecular theories are able to simultaneously capture tube dynamics at both slow shear rates dominated by reptation, $\dot{\gamma} < \tau_d^{-1}$, and at intermediate rates dominated by CCR, $\tau_d^{-1} < \dot{\gamma} < \tau_R^{-1}$; where τ_R is the rotational Rouse time assumed to govern tube stretching. At shear rates fast enough for tube stretching to dominate $\dot{\gamma} > \tau_R^{-1}$, agreement has been only partial even for the bulk rheological response and has consistently been shown to diverge from experimental results at increasing shear rates. Two possible reasons have been suggested for this disagreement. The first is the realization that, at some point under large enough shear rates, the tube may stretch sufficiently to diverge from the simple linear Rouse entropic elasticity into a more realistic finitely extensible spring with a nonlinear force-extension curve.[22] Incorporating any nonlinear spring into an analytically tractable theory while retaining all other desirable dynamics is difficult and would necessitate the inclusion of perhaps questionable closure approximations.

The second possibility is the failure of the pre-averaging approximation itself. The pre-averaging approximation has been the key enabling assumption of all molecular theories and a central issue of debate in the field for over 30 years.[23] For the pre-averaging approximation to hold, one must assume that, at any given instant, all molecules take on similar conformations within the fluid, that is, the conformational distribution must be kept narrow. As an example, one proposed form for the relationship between molecular conformation and, τ_{ij}^p, the polymer stress tensor was:[16,18]

$$\tau_{ij}^p = \frac{c}{N}\frac{3kT}{a^2}\int_0^Z \left\langle \frac{\partial R_i(s)}{\partial s}\frac{\partial R_j(s)}{\partial s}\right\rangle \mathrm{d}s \qquad (1)$$

Here, c/N is the polymer chain concentration, k is Boltzmann's constant, T is the temperature, a is the tube diameter, Z is the number of entanglements per chain, and $R(s,t)$ is the orientation of entanglement segment s at time t, which contains the full molecular conformation information in all vectorial directions i and j. Notice that the integrand, the so-called chain-tangent tensor correlation function, is a bracketed quantity denoting an average over all chains in the solution. For eq 1 to be exact, the time evolution describing the bracketed quantity must be linear. Linearity, however, is approached only at less than unity dimensionless deformation rates. For larger than unity deformations rates, the equation may remain approximate if the width of the distribution of chain conformations is narrow. If the distribution is broad, then, for instance, the tail of the distribution may account for a disproportionately large amount of the stress, thus rendering the pre-averaged quantity insufficient for an accurate representation of material properties. Unfortunately, to find useful quantities such as the stress tensor and the structure factor, theories must be formulated with respect to the average chain description (e.g., the bracketed quantity) to obtain closure for such an analytical solution, whereas in actuality, material properties arise from the collective effects of many chains, each with its own stochastic variation.

As pointed out by McLeish, the errors introduced by the pre-averaging approximation in entangled systems may not be as large as in dilute systems.[23] Because the deformations of dilute, free-floating polymers are strongly influenced by hydrodynamic drag, conformations near full extension are not uncommon even under moderate velocity gradients.[24−27] Entangled polymers, on the other hand, are topologically constrained, and shear rates in the $\dot{\gamma} < \tau_R^{-1}$ range are arguably not great enough to create large deformations. The situation under significantly larger shear rates, however, may be different. Stochastic computer simulations by Read have already hinted at the possibility that these distributions may be rather broad.[23]

To date, the distribution of entangled polymer conformations remain unknown. Molecular-scale experimental probes such as birefringence and neutron scattering have revealed a wealth of information about conformational orientation and anisotropies under controlled flow conditions and a range of time-scales.[19−21,28−34] Nevertheless, these methods continue to be limited to measuring an ensemble of chain conformations, thus precluding any information on individual chains or the conformational distributions throughout the fluid. Alternatively, a direct visualization of single-polymer molecules using video microscopy techniques can remove the aforementioned limitation.

In this paper, we have used the single-molecule approach to determine these molecular conformations as well as its dynamics. In the past, single-molecule video microscopy was used to test reptation autodiffusion scaling predictions at equilibrium,[35] and in a landmark study by Perkins et al., where chain retraction inside a "tube" was visualized for the first time.[36] In that work, optical tweezers were used to stretch DNA polymers while only momentarily perturbing background chains. In the present work, the situation is different. Here, instead, we ask ourselves what the effects of bulk flow deformations on single chains are. In this way, both measured and background chains are deformed, mirroring the situation in actual flows. In the present study, the dynamics in shear flow is investigated. Of all flow types, shear flow has historically been the most difficult test for entangled polymer theories, particularly for nonlinear deformations.[6−8,11,15,18]

In the first sections of this paper, we describe the sample preparation, optics, and the shear flow apparatus. Next, we present extensive rheological characterizations of four polymer solutions of varying concentrations, from semidilute to well-entangled. We then show the results of single-molecule measurements of identical samples subjected to three shear flow histories: (i) the relaxation following the cessation of a fast shear flow, (ii) deformation through a range of steady shear rates, and (iii) the transient deformation response to the sudden inception of shear flow. Finally, we show a brief comparison to the ROLIE-POLY theory.[37] As we shall see, the results of

the present study call into question the validity of the preaveraging approximation in fast shear flows and provide other useful insights into the behavior of entangled polymers.

Entangled Sample Preparation

The aim of this study is to observe the conformations that entangled polymers adopt in shear flow. To accomplish this, we sought to prepare an entangled and spatially homogeneous solution of monodisperse, linear DNA in which a small fraction (of order 10^{-4}) of the chains was fluorescently stained. (In this approach, the stained and, thus, visible chains are the "test" chains, while the neighboring unstained, invisible chains formed the confinements.) Our starting point was commercially available λ-phage DNA (48.5 Kbp). We then developed a technique to increase and control the concentration from the purchased stock vial to enable experiments at different entangled concentrations. λ-phage DNA from Invitrogen was shipped in a 10 mM Tris-HCl (pH = 7.4), 0.1 mM EDTA, and 5 mM NaCl buffer solution. To eliminate electrostatic effects, the negative charge of the DNA backbone had to be effectively screened by counterions in solution, mostly Na^+. A previous experiment by Smith et al. had obtained diffusivity data for different concentrations and DNA lengths at equilibrium and found good agreement with scaling laws derived from reptation arguments.[35] That study used 2 mM NaCl for 0.63 mg/mL of λ-phage DNA. In our experiments, reported here, we maintained the NaCl concentration between 5 and 10 mM. With these counterion concentrations, we expect that electrostatic effects will not interfere with results. EDTA was sometimes added (approximately 2 mM) to enhance the stability of DNA by reducing the activity of any enzymes that might be present in solution.

Prior to concentrating the stock DNA, target concentrations were expressed in terms of c^*, or the concentration at which isolated coils begin to overlap. The target concentration was then converted to a mass per volume basis by multiplying the value of c^*. The value of c^* was calculated for our unstained polymers comprising the background tube chains by rescaling diffusivity data from stained, isolated chains.[38] In this separate single-molecule study, the diffusivity of TOTO-1 stained λ-phage DNA was measured at $D = 0.47\ \mu m^2/s$ in a $\eta = 0.95$ cP solvent viscosity. This result was then used to estimate a radius of gyration of $R_G = 0.73\ \mu m$ using Zimm's model for θ solvent conditions: $R_G = 0.196\ k_BT/\eta\sqrt{6}D$ and $T = 297$ K. From this, we rescaled the diffusivity for the persistence length, P, of the native state from the stained chain using $D \propto P^{-2/5}$. This gave for the native chain $D = 0.59\ \mu m^2/s$ and $R_G = 0.58\ \mu m$. Then the coil volume, $v_{coil} \approx 4/3\pi R_G^3$, was calculated to be $c^* = v_{coil}^{-1}\ (M/N_A) = 0.064$ mg/mL, where $M = 32$ MDa for λ-phage DNA and N_A is Avogadro's number.

Four DNA concentration ranges were investigated: 10 (0.65 mg/mL), 16 (1.0 mg/mL), 23 (1.5 mg/mL), and 31−35 c^* (2.2 mg/mL). The concentration step was accomplished via centrifugation against a porous membrane (Microcon, Centricon, or Centriplus depending on the initial volume; Millipore Corporation). The membrane was rated for a cutoff of 100 kDa. Even though λ-phage DNA is approximately 320-fold larger, it is also flexible and roughly 10% was lost through the membrane regardless of the target concentration. All other buffer species are particles smaller than the cutoff and are not concentrated in this procedure. Initially, when concentrations are low, the centrifugal acceleration was kept around 1000 g to minimize DNA loss. After every 15−30 min of centrifugation, the retentate vial was weighed to estimate its concentration and the rotation speed was ramped up to a final value of 2000−2200g for targets of 1.0 mg/mL and higher. According to the manufacturer, accelerations up to 14000g have been tested, and no damage was detected in long DNA. Using this procedure, final concentrations of up to 2.2 mg/mL (35 c^*) have been obtained. To recover the concentrated DNA the retentate vial was inverted into a second vial and spun at 1000g for 2 min.

According to simple scaling laws, the intrinsic timescales of the fluid are greatly affected by even small inhomogeneities in concentration. After centrifugation, however, the concentrate was visibly inhomogeneous due to the formation of a DNA mass gradient along the acceleration direction. Before homogenization, the solution was heated to 65 °C for 10 min to melt the end overhangs. After being quickly cooled back to room temperature, the chains were linear and could move freely, thus promoting mixing. When done without this heating step, the homogenization step (discussed below) gave poor results even after very long times. Next, to accomplish homogenization, we tumble-mixed the sample at roughly 4 rpm for 5 min and quickly followed by placing the solution in a water bath at 55 °C for another 5 min. This process was repeated over the course of 3−5 h. Finally, the sample was allowed to tumble-mix overnight at room temperature.

The efficiency of our mixing protocol and the resulting concentration homogeneities were independently verified using confocal microscopy. In this test, a ∼10-fold higher fraction of stained λ-phage DNA was added to an unstained solution at 16 c^*. The mixture was then slowly pipetted up and down a mere 20 times with a wide-bore tip. Notice that this is a much weaker mixing protocol than the repeated tumble-mixing and heating cycles followed by overnight tumbling used in all rheology and single-molecule experiments. The resulting solution was then placed on a slide and imaged under a confocal microscope (Nikon Eclipse E800 and Radiance 2000). The confocal optical setup was necessary in order to isolate a horizontal slice of solution thin enough (∼1 μm) to visualize several hundred, but spatially separated stained molecules per image. Using an ordinary microscope would have produced a depth-averaged image resulting in uniform background brightness that is insensitive to concentration inhomogeneities. The confocal images, on the other hand, could capture any inhomogeneities unambiguously, as evidenced by polymer clusters still present in preparations with fewer pipettings. Images (Figure 2 in the Supporting Information) showed stained molecules uniformly interspersed among unstained ones, i.e., a well-mixed solution.

With a homogeneous solution in hand, we proceeded with characterization. The final concentrations were measured with an UV−vis spectrophotometer after a 1:50 dilution of a minute but reproducible sample amount in an identical buffer. For very high or low concentrations, the dilution ratio was slightly adjusted to keep the absorbance between 0.1 and 0.9 for accuracy. It was important to also let this preparation tumble-mix and heat for at least 1 h to ensure accurate dilution. The 260 nm line absorbance was measured at room temperature, and an extinction coefficient of $\epsilon = 20\ g^{-1}\ cm^{-1}$ L for DNA was used to estimate the final concentration. This was repeated at least three times to minimize cuvette dilution effects and ensure consistent results. Measuring the concentration on the day of the bulk rheology measurements helped ensure that the DNA samples were truly well mixed.

Another important characterization step was to check our solutions for polymer fragmentation during sample preparation and the experiment itself. This was accomplished in two separate experiments: by gel electrophoresis and by visualization of single coil sizes. Gel separations were run for both unmodified

stock solutions and final concentrated samples for all preparations used in this study. A low-range DNA ladder containing fragments of 1 Kbp up to 97 Kbp (Invitrogen) was also co-run to guarantee the gel's ability to detect any fragments. Gels showed an absence of any fragments (<48.5 Kbp pieces) for all preparations. An example of this is shown in Figure 3 of the Supporting Information. The band smear toward longer DNA sizes (slower mobilities) seen in concentrated separations was presumably due to entanglements in the sample, causing some molecules to migrate as aggregates, and has no bearing on detecting fragmentation. It was also essential to verify the possibility of DNA cleavage by the single-molecule shear apparatus (described below). This case was tested by subjecting the highest entangled concentration (35 c^*) to sample loading onto the apparatus, continuous shearing at the highest shear rate setting for 30 min, and unloading. The recovered solution was then gel-separated against the initial stock sample. This scan also showed identical migration and no signs of fragmentation. As a qualitative test for DNA robustness in entangled solutions, gels were also run after vigorous and extensive pipetting with a wide-bore tip. Again, no fragments were detected. The lack of fragmentation was also verified via direct single-molecule visualizations. Molecules from entangled preparations were diluted and stained as usual. Under a microscope, they were checked for coil size and brightness and presented narrowly peaked distributions, as expected, demonstrating no fragmentation beyond that already present in stock solutions (<5%). Finally, no fragments were observed among stained molecules during the actual single-molecule experiments.

After characterization, we prepared the solvent environment to receive stained DNA molecules and enable its visualization for long time periods by preventing photocleaving and nicking. First, β-D-glucose was added to a final concentration of 1% (w/w). Subsequently, β-mercaptoethanol, glucose oxidase and catalase were added using an identical procedure to the dilute case but with different mixing times. While molecules smaller than the packing length of mesh of entanglements, such as β-mercaptoethanol or even catalase, need only 5−15 min to mix, stained DNA mixing times are highly dependent on concentration and require 15 min (for $\approx$ 0.65 mg/mL) and much longer for higher concentrations. Unfortunately, after addition of the glucose oxidase/catalase oxygen-scavenging mixture, the solution pH will quickly drop because O_2 molecules readily diffuse into the low-viscosity aqueous solution, resulting in the release of protons from the reaction mixture. If the pH is allowed to drop below ~3, fluorophores become too dim to yield a useful signal. For these reasons, the mixing time for stained DNA was minimized and the final preparation was promptly loaded into the apparatus and shielded from air with a layer of mineral oil. This step typically took less than 2 h. DNA was stained with YOYO-1 dyes (Molecular Probes) using the same procedure as previously reported.[24,27]

Optics and Imaging

The optical setup was identical to that reported in our previous experiment.[27] Briefly, imaging and detection was done by an inverted homemade epifluorescence microscope coupled to a CCD camera (Micromax, Roper Scientific, Trenton, NJ). Molecules were epi-illuminated by a 100 W mercury arc lamp (100HBOW/2, Zeiss, Thornwood, NY) after a 480 ± 20 nm bandpass excitation filter and a 505 nm long pass dichroic mirror. Light was collected by a 1.45 NA, 63× oil immersion Planapo objective (Olympus, Melville, NY) with a 535 ± 25 nm emission filter (Filter set 41001, Chroma, Brattleboro, VT) and a 300 mm achromatic doublet tube lens (Newport, Irvine, CA). Pixels were binned 2 × 2, giving 0.27 μm × 0.27 μm superpixels. Images were sampled at 10 Hz.

Shear Flow Apparatus

A custom-made apparatus was built to enable the simultaneous generation of controlled shear flows and visualization of the entangled dynamics of single molecules. This apparatus allowed observation of the flow-vorticity plane of shear flow (as opposed to the flow-gradient plane visualized in our previous work[27]). Similarly to a previous shear apparatus built in our lab[26,39] (a picture is available elsewhere[40]), our new device employs only one moving shear wall while tracking the molecule of interest by counter translating the entire assembly. However, to improve our previous device, a longer shearing wall and sample holding pool was used to increase the maximum amount of applied strain (in total translation range of the shearing wall divided by gap separation, $\bar{\gamma} = \gamma/h$) without sacrificing the gap separation or increasing the required sample volume. The maximum applied strain was $\bar{\gamma} \approx 650$. The simplicity of this design (with removable pieces and a minimum of moving parts) also made it easier to operate: assembly, disassembly, cleaning. and storage typically took <1 h.

A schematic of the apparatus can be seen in Figure 1. The flow-vorticity shear flow apparatus rested on the stage of an inverted epifluorescence microscope. The bottom horizontal shearing wall was a thin coverslip window though which polymers were also imaged. This surface was fixed with respect to the rest of the apparatus. Two thin sheets of mica were glued to each side of the bottom coverslip/shearing wall, forming a long channel with a rectangular cross-section about 1 cm wide. The mica sheets kept a constant gap separation of $h = 75$ μm between the bottom wall and the movable shearing wall resting horizontally above the mica. Plexiglas walls were placed around this assembly to contain the DNA solution (called the DNA "pool"). The minimum sample volume was $\approx$ 600 μL. A feedback-controlled motor (Oriel) was used to move the top shearing wall at a constant velocity, v, relative to the fixed bottom coverslip, thus generating a constant applied shear rate of $\dot{\gamma} = v/h$. A spring-loading force was applied downward on the top wall and against the spacers to keep the gap separation from fluctuating during translation, therefore stabilizing the flow. To track the molecule of interest, a second feedback-controlled motor was used to translate the microscope stage and, with it, the entire apparatus in the opposite direction of shearing. To compensate for molecular diffusion, the experimenter adjusted the speed of the second motor and the focal distance in real time.

Because the apparatus was of a new design, extensive characterizations were necessary to verify the quality of the shear flow before attempting single-molecule measurements. As in previous work,[24,26,27] the motion of fluorescent spheres in a high viscosity sucrose solution was used to fully reconstruct the generated flow-velocity field. The following flow characteristics were verified: linearity and reproducibility of the full three-dimensional shear flow geometry and between right and left shearing translations, reproducibility of shear rate for different motor settings, reproducibility of the gap separation (measured both visually and indirectly via the shear profile) between disassembly and reassembly of the apparatus, temporal stability (noise and drift) of the shear rate, and gap alignment. As an overall final check, a series of dilute shear experiments were performed to measure the mean fractional extension of λ-phage DNA as a function of the Weissenberg number, $Wi = \dot{\gamma}\tau$, where τ is the longest polymer relaxation time also measured with

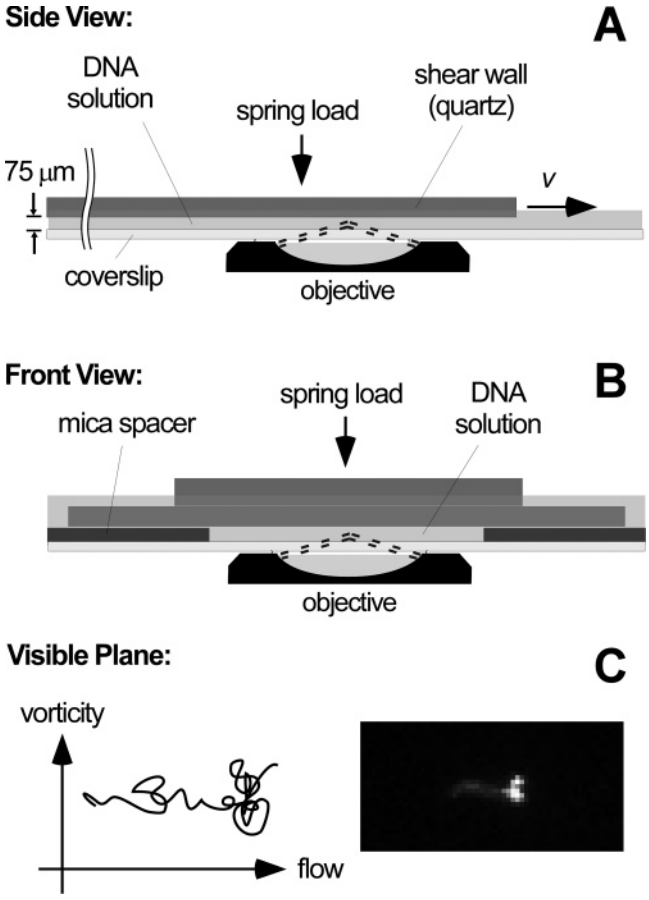

Figure 1. Schematic representation of the flow-vorticity apparatus (not to scale). (A) Side view showing the fixed and moving shear walls separated by $h = 75\ \mu$m by two mica sheets (shown in B). The applied shear rate is the shear wall translation speed, v, divided by the gap separation, or $\dot{\gamma} = v/h$. The polymer solution (light gray) flows inside the gap and is contained by four exterior walls forming the sample "pool" (not shown). The gap is stabilized by spring loads pressing downward against the shearing wall. The whole assembly sits over the stage of an inverted microscope. The bottom, fixed shear wall right above the microscope objective (1.45 NA) is an optically transparent coverslip through which images are acquired in real time. (B) Front view of the same assembly shown in (A). Here the mica spacers are shown holding the sides of the moving shear wall at a constant gap distance from the coverslip at the bottom. The top shear wall moves in and out of the plane of the paper. The shearing wall is shallower on both sides to provide external backflow channels that minimize perturbations to the shear flow inside the gap. (C) Image plane made visible with the flow-vorticity apparatus and an image of an actual entangled polymer in shear flow (35 c^* and $\dot{\gamma} = 1.3\ s^{-1}$).

this apparatus. The resulting curve faithfully reproduced previous data from both Smith et al.[26] and Teixeira et al.[27] This result, along with the full set of validation tests, is detailed in the Supporting Information. After this, the apparatus was considered to be ready for experiments employing entangled DNA solutions.

Rheology

Before single molecules were visualized in our apparatus, the DNA samples were subjected to a series of rheological characterizations. Because the solutions for both the rheological measurements and the single molecule visualizations were prepared in an identical manner, molecular conformations could be related to bulk viscoelasticity directly and unambiguously without the need to introduce any assumptions or rescaling. Thus, this unabridged correspondence between macroscopic mechanical measurements and microscopic conformation measurements could provide useful benchmark data for future studies. Another key motivation was to ascertain if λ-DNA could display the characteristics unique to entangled polymer samples and whether its behavior would be similar to that of entangled synthetic polymers, and if so, above what concentration was this behavior reproduced. It is not known a priori whether DNA solutions should behave similarly to their synthetic counterparts even though previous measurements have shed some light on this question.[41−43] DNA possesses a much more complex chemistry than virtually any synthetic polymer. It is a much thicker and stiffer polymer, and its ratio of persistence length to hydrodynamic radius is much larger. Our main motivation in drawing this comparison, as stated previously, is that synthetic polymer solutions are involved in several important industrial processes, and so they have been the main modeling targets for constitutive equations derived from molecular models.

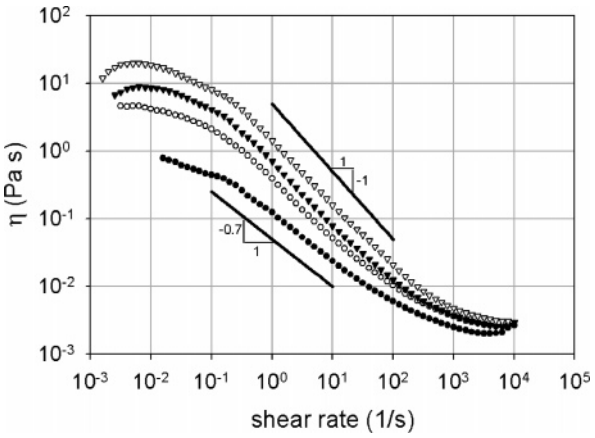

Figure 2. Shear viscosity, η, as a function of steady shear rate for several λ-DNA concentrations. Lines with slopes of -1.0 and -0.7 have been added to examine the intermediate frequency power-law behavior of the highest and lowest concentrations, respectively.

To perform this bulk rheological characterization, a cone and plate Ares rheometer (Rheometric Scientific) was used in conjunction with a water bath to maintain the temperature at about 18 °C. Four samples were prepared, as mentioned before, and their concentrations were approximately 10, 16, 23, and 31 c^*. It must be noted that previous experiments[35] have shown that the diffusivity of concentrated DNA follows reptation-based scaling ($D \sim c^{-7/4}$) for concentration as low as 0.63 mg/mL ($\sim$10 c^*, i.e., the lowest concentration investigated in this paper).[48−51] Note that, in the results presented, no shift factors were introduced other than when explicitly mentioned.

Figure 2 depicts viscosity thinning profiles for the four concentrations investigated in this paper. The shear thinning exponent varies from -1.0 for the highest concentrations to -0.7 for the lowest. An exponent of -1.0 seems to be the apparent limit for well-entangled solutions, and similar scalings have been measured in synthetic systems.[45−47] In relation to theory, the reptation model proposed by Doi and Edwards predicts a thinning exponent of -1.5.[7] This discrepancy has been attributed to constraint release (CR),[77] mentioned previously, which releases topological constraints on polymers due to relative motion between chains. So our data seems to suggest that, like synthetic polymer systems, DNA, a stiff biomolecule, also experiences nonreptative phenomena (CR). Furthermore, it is known that dilute polymer samples exhibit a shear thinning exponent of -0.5, indicating that the samples, especially the ones with the highest concentrations, are well within the entangled regime.

Another measure that can be used to characterize the extent of entanglement of a polymer solution is the number of

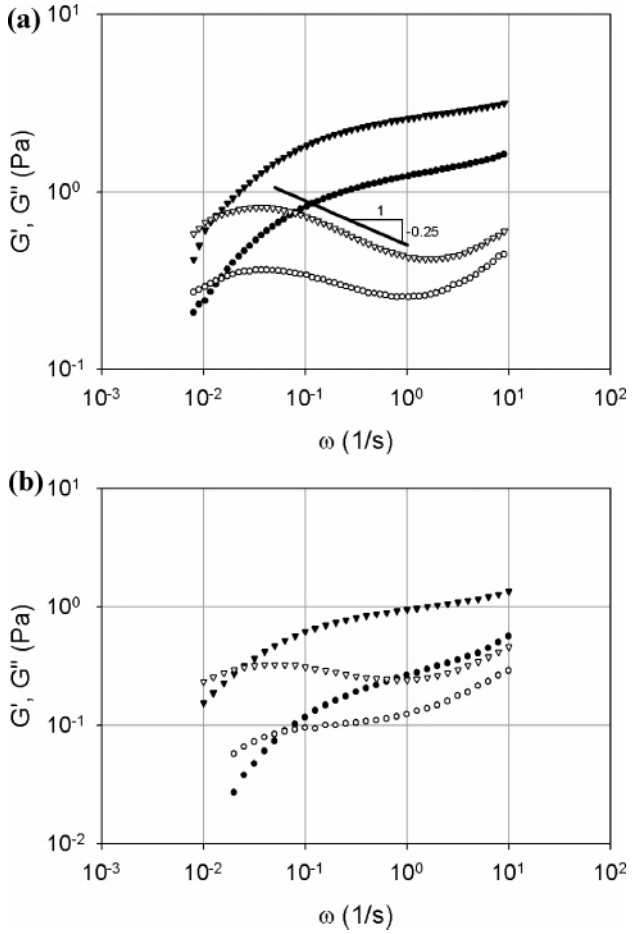

Figure 3. (a−b) Linear oscillatory shear response of entangled λ-DNA solutions for 10 (bottom, circles), 16 (bottom, triangles), 23 (top, circles), and 31 c^* (top, triangles). Open and closed symbols represent G' (storage modulus) and G'' (loss modulus), respectively. These, as well as all other bulk and single-molecule experiments were carried out at $T = 18$ °C. The line with a slope of $-1/4$ has been added to analyze the scaling for the decay in the 35 c^* loss modulus at intermediate frequencies.

entanglements per molecule (N_e). This value can be extracted from the plateau modulus ($G_N^{(0)}$) via Ferry's "temporary network" formula: $N_e = [(4/5)(\rho RT/G_N^{(0)})]^{-1}$ M. $G_N^{(0)}$corresponds to the value of the storage modulus (G') at its plateau, an approximately flat region at intermediate frequencies ($\tau_d^{-1} \leq \omega \leq \tau_R^{-1}$). Parts a and b of Figure 3 clearly depict the development of this plateau as the concentration increases to 31 c^*. $G_N^{(0)}$ is estimated to be approximately 2.7 Pa, yielding $N_e \sim 22$, another indication that the solutions are well-entangled. The loss (G'') and storage modulus curves are useful also because they provide valuable information regarding the intrinsic time scales and phenomena that govern the internal dynamics of polymer systems. The frequency at which the curves cross is said to be approximately the inverse of the disengagement time (i.e., the longest intrinsic time scale for entangled polymer solutions).[77] As expected, the crossover frequency decreases as the concentration increases, indicating an increase in the terminal relaxation time. For the three highest concentrations, the data yields $\tau_d \sim c^{0.43\pm0.04}$. The lowest concentration had a much lower disengagement time than that predicted by this scaling. The curves for G' and G'' have other features characteristic of entangled polymer solutions as well. The plateau in the storage modulus, at intermediate frequencies, for the highest two concentrations is one such classic feature. Even though their plateau is not perfectly flat, we can estimate $\tau_d \sim O(10^2)$. Usually, the moduli

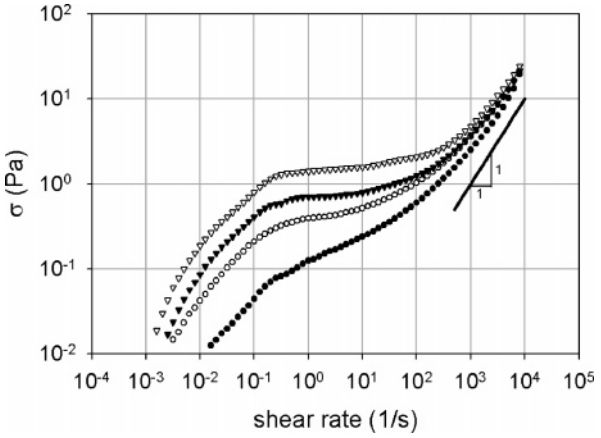

Figure 4. Shear stress as a function of steady shear rate for several λ-DNA concentrations. Terminal scaling of 1.0, at high shear rates, is shown.

start to increase with a slope of a $1/2$ at very high frequency. The onset of such a behavior is said to happen at the inverse of the Rouse time for an entanglement strand[7] (τ_e), the piece of the polymer chain between successive entanglements. The Rouse time for the polymer itself can then be calculated[76] as $\tau_R = Z^2\tau_e$. Our curves, at the highest concentrations, do not exhibit such a slope, presumably because we did not probe high enough frequencies. Thus, a decent estimate of the polymer's Rouse time cannot be made. Another feature is the dramatic decrease exhibited in the loss modulus (the local maximum and minimum differ by a factor of about 2 for the 31 c^* loss modulus curve). The frequency range corresponding to this reduction is about the same as that corresponding to the plateau in the storage modulus. The original Doi−Edwards reptation concept did predict such a drop; however, the rate of decrease was overpredicted to be $G'' \sim \omega^{-1/2}$. Recent studies that include contour length fluctuations (the fast process where the chain ends contribute to overall stress relaxation by quickly relaxing their local conformation) have refined the exponent to be about $-1/4$.[76] Figure 3a clearly shows that, at the highest concentration, the dynamic loss modulus for our DNA samples does decrease with a decay exponent of about $-1/4$; at lower concentrations, the decay rate decreases. This implies that contour length fluctuations do seem to play a significant role in DNA dynamics at high concentrations.

Another quantity that was obtained was the steady shear stress as a function of shear rate, shown in Figure 4. Qualitatively, the curve looks very similar to the 31 c^* storage modulus and has two important features that must be noted. First is the presence of a plateau for intermediate shear rates. Such a plateau is not observed in dilute polymer solutions. Interestingly, reptation-based theories actually predict shear thinning for this intermediate region. However, certain nonreptative phenomena (constraint release mechanisms for example) start becoming nonnegligible at these intermediate rates and help relieve some of the stress in the system, alleviating any instability in shear stress and generating a plateau.[77] Second, we can see that, at high frequencies, $\sigma \sim \dot{\gamma}$. Nonreptative processes may again be responsible for this upturn in shear stress at these high frequencies. Strong flows are able to stretch polymer molecules and thus add to the stress measured.[23] In addition, convective constraint release is believed to induce "kinks" along a chain's contour due to the removal of adjacent constraints/chains. These kinks misalign different parts of the chain, and velocity gradients are thereby able to induce stress in the polymer system. Certain models[23] that include convective constraint release and chain

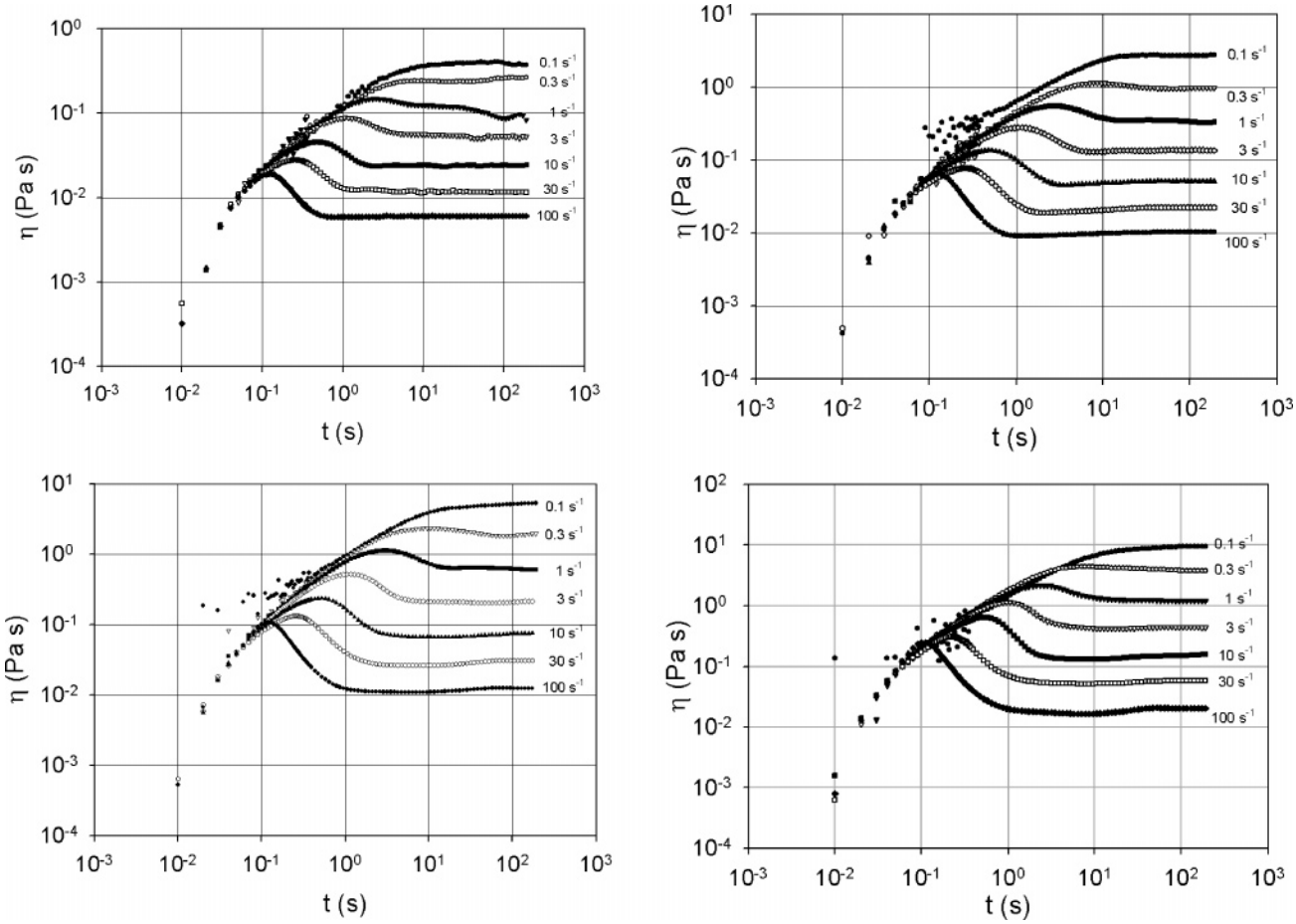

Figure 5. Transient response in viscosity following a sudden inception of shear flow to entangled λ-DNA solutions initially at equilibrium. Different curves represent different shear rates (indicated in the graphs).

stretch predict increasing shear stress with $\sigma \sim \dot{\gamma}^{1/2}$, but we see a stronger dependence than this. As mentioned previously, it is possible that, at the high strain rates probed (well in excess of the Rouse time by any estimate), the worm-like nature of DNA manifests itself, resulting in a greater stress than that predicted by theories using Hookean approximations. Recently, simulations incorporating finitely extensible springs have been performed for entangled polymer systems.[78] However, to date, they have not been able to accurately capture all of the dynamics at high frequencies. Schieber and co-workers were able to predict $\eta \sim \dot{\gamma}^{-0.87}$ for steady shear flow. The viscosity scaling agrees favorably with our results. Despite these attributes, the same simulations were not able to capture the upturn in dynamic moduli at high frequency.[78]

Moving away from steady measurements, parts a−d of Figure 5 depict the time-dependent shear viscosities for our samples. All the samples exhibit an overshoot at $\dot{\gamma} \sim O(10^{-1})$. Conventional understanding of this phenomenon is that overshoots occur when the time scale of flow-induced deformation is similar to the intrinsic terminal time scale. At such relatively strong flows, the perturbation to a polymer's orientation and affine deformation leads to the observed overshoot in viscosity before relaxing to its steady-state value.[52] For lower shear rates, the viscosity monotonically increases to its steady value. In our case, these transient measurements would imply $\tau_d \sim O(10)$, an order of magnitude lower estimate than that obtained via Figure 3. Surprisingly, a similar misestimate for polymer time scales using normal stress differences has been noted for synthetic polymers.[52]

From the transient shear data, we can see that the time at which the viscosity peaks, τ_{peak}, reduces as the shear rate is increased. This is in accordance with the available understanding because entangled solution theory suggests that the overshoot should occur at a fixed value of strain (i.e., $\tau_{peak} \sim \dot{\gamma}^{-1}$) for flow strengths low enough not to induce chain stretching.[52,53,77] McLeish reports that, for $\dot{\gamma}\tau_R \geq 1$, the stress peak time remains at approximately the Rouse time but the stress maximum grows.[23] We do find a continually growing maximum stress but do not observe a saturation of the peak time. To quantify the relation between the peak time and the shear rate, nonlinear fitting was employed. From our data, we find that the exponent (i.e., "b" in $\tau_{peak} = a\dot{\gamma}^b$) actually varies from -0.96 ± 0.079 at the highest concentration to -0.83 ± 0.042 at the lower concentrations. This relation extends over the entire range of shear rates, where a peak is observed. The peak strain does start at approximately 2−3 and then increases with strain rate as predicted by theory.[77]

Finally, the nonlinear relaxation modulus was measured by quickly imposing a strain of 13 units and watching the relaxation as a function of time. Figure 6 reveals that all the samples seem to have two major contributors to the overall relaxation process. There is a fast, initial relaxation process, which is attributed to constraint release events that take place due to chains retracting to their equilibrium length (lasts for approximately 0.1 s). Later, a slower relaxation process, reptation, takes over. This general shape of the nonlinear modulus is qualitatively the same as that predicted by theory and has been widely observed.[7]

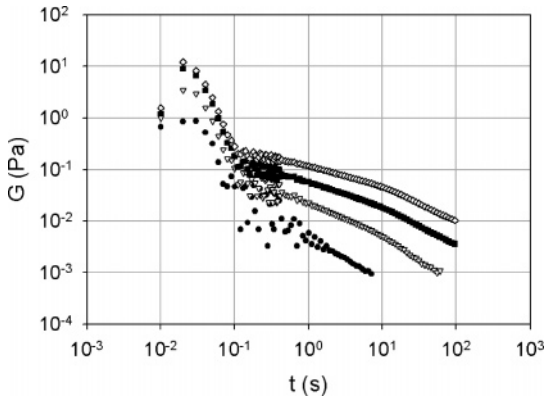

Figure 6. Nonlinear modulus, $G(t)$, is shown for several stress relaxations after a step shear of 13 strains at $\dot{\gamma} > 1000\ s^{-1}$. The four λ-DNA concentrations are shown.

In conclusion, from the rheological measurements, both 23 and 31 c^* solutions could be considered well-entangled from both their linear and nonlinear rheologies. They both had a steep -1.0 decay in shear viscosity and a plateau in shear stress lasting two or more decades in shear rate. Those concentrations also displayed a local minimum in G''. The 16 c^* solution, while not strictly well-entangled, could be considered entangled as it did show undershoots in startup shear. The lowest concentration investigated here, 10 c^*, while found to be sufficiently concentrated for reptation scaling arguments based on the equilibrium center-of-mass diffusivity,[35] could not be considered an entangled solution as it did not display an undershoot in viscosity for the startup of shear. Furthermore, its viscosity power-law decay exponent of -0.7 was roughly halfway between the dilute (-0.5) and well-entangled (-1.0) behaviors. Therefore, we conclude that 10 c^* fell near the boundary between semidilute and entangled. These characterizations will be compared later to the dynamics of single chains.

Extension Relaxation

With the rheological characterization completed, we moved to single-molecule measurements. In the first of these experiments, we examined the extension relaxation of chains after the cessation of a fast shear flow. To recall, in all single-molecule measurements included in the present study, an order 10^{-4} of λ-phage DNA polymers were stained and mixed in the unstained and therefore invisible monodisperse and entangled solution. In this way, the stained and visible chains consisted of our test chains, while the neighboring unstained and invisible chains formed the confinements. Apart from for the presence of fluorophores in the stained chains, which increased their persistence and contour lengths by $\approx 35\%$, the test and tube polymers were identical. For the extension relaxation experiments, test chains were initially allowed to equilibrate by letting the solution rest for a time period of 10 times the full relaxation cycle, from partially extended to coiled. A spring-loaded trigger mechanism coupled to the shearing wall was used to apply 13 strain units (1 mm translation) in approximately 0.01 s (estimated from the spring constant). This resulted on an average shear rate of over $1000\ s^{-1}$, which would have been more than enough to stretch the same polymer in a dilute solution at the same solvent viscosity ($\dot{\gamma}\tau > 100$),[26,27,39] thus qualifying as essentially an "instantaneous shearing".

All extension relaxation trajectories were visually synchronized to $t = 0$ at the end of shearing. Movies were recorded at 10 frames/s; therefore, the error in time synchronization was at most ± 0.05 s. The flow-projected maximum extensions of individual polymers, x, or the distance between the leftmost and rightmost segments in the flow direction, were measured for each movie frame with custom semiautomatic image analysis software. Figures 7 (ABC) shows several trajectories of individual fractional extensions, x/L (light-gray lines), where the extension, x, was normalized with the contour length, $L = 22\ \mu$m. The experiment was performed for the three highest concentrations: 16 (A), 23 (B), and 35 c^* (C). The average trajectories are overplotted as black circles.

According to the accepted theoretical notion, we should expect entangled chains to undergo two distinct relaxation phases. Initially and right after a fast deformation, the chain is highly stretched and quickly retracts to fill the diameter of the confining tube.[23] This time scale is taken to be the rotational Rouse time, τ_R, which is the longest characteristic time of an identical, hydrodynamically non-self-interacting (free-draining) polymer in a dilute environment. This implies that the presence of the tube around the chain is assumed to incur a negligible effect in the initial retraction. After filling the tube, the polymer cannot retract any further but still retains an oriented state over length scales of the entire chain because the tube itself was oriented by flow. This state then relaxes as chain segments diffuse or *reptate* out of the original tube into a new and more randomly oriented tube. The reptation process is much slower than the initial Rouse retraction and much more sensitive to polymer concentration, $\propto c^{\beta}$, where β has taken values of 1.5 up to 3 for different scaling derivations and rheology measurements.[48,54−56] The reptation time scale is often termed the disengagement time, τ_d, or the time it takes for the test chain to reptate out or disengage from its original tube.[7] This relaxation mode is aided by the contour length fluctuations (CLF), or "breathing modes" of neighboring chains.

To extract the intrinsic time scales from single-molecule relaxations, the average trajectories (black circles) were numerically analyzed using a Levenberg−Marquardt nonlinear least-squares fitting algorithm.[57] We fitted the data to a constant plus single (dark-gray lines) and double (gray lines) exponential decays of the form: $x^2(t) = A + B\exp(-t/\tau_{fast}) + C\exp(-t/\tau_{slow})$. Here, x is extension and t is time, as before, while A, B, C, τ_{fast}, and τ_{slow} were simultaneously fitted. The fits shown in Figure 7 were made to the unsquared extension for the presentation purposes, whereas characteristic times were calculated for the squared quantity to maintain consistency with the methodology used in past single-molecule relaxation measurements. For the 16 c^* sample (A), there was almost no appreciable difference between single and double exponential fits, although the latter was slightly more adequate. For the next higher concentration, 23 c^* (B), two distinct time scales emerged. Here, a single relaxation time was unable to reproduce the average trajectory accurately, whereas a double exponential gave a good fit. For the highest concentration, 35 c^* (C), the two time scales became well separated and the decay clearly could not be reproduced by a single exponential. In summary, we found $\tau_{fast} = 1.7$ s and $\tau_{slow} = 10$ s for the 16 c^*, $\tau_{fast} = 2.2$ s and $\tau_{slow} = 24$ s for the 23 c^*, and $\tau_{fast} = 1.7$ s and $\tau_{slow} = 92$ s for the 35 c^*. In comparison, the long time estimate from bulk measurements is 78.55, 68.82, and 58.86 s for 31, 23, and 16 c^*, respectively. Qualitatively, the long relaxation times are of the same order of magnitude and the relative error decreases as the concentration increases.

Our data suggests that τ_{fast} remained roughly constant at 2.0 ± 0.5 s. Qualitatively, this is consistent with the theoretical picture. Quantitatively, on the other hand, this value seems much larger than the theoretical rotational Rouse, τ_R, assumed to

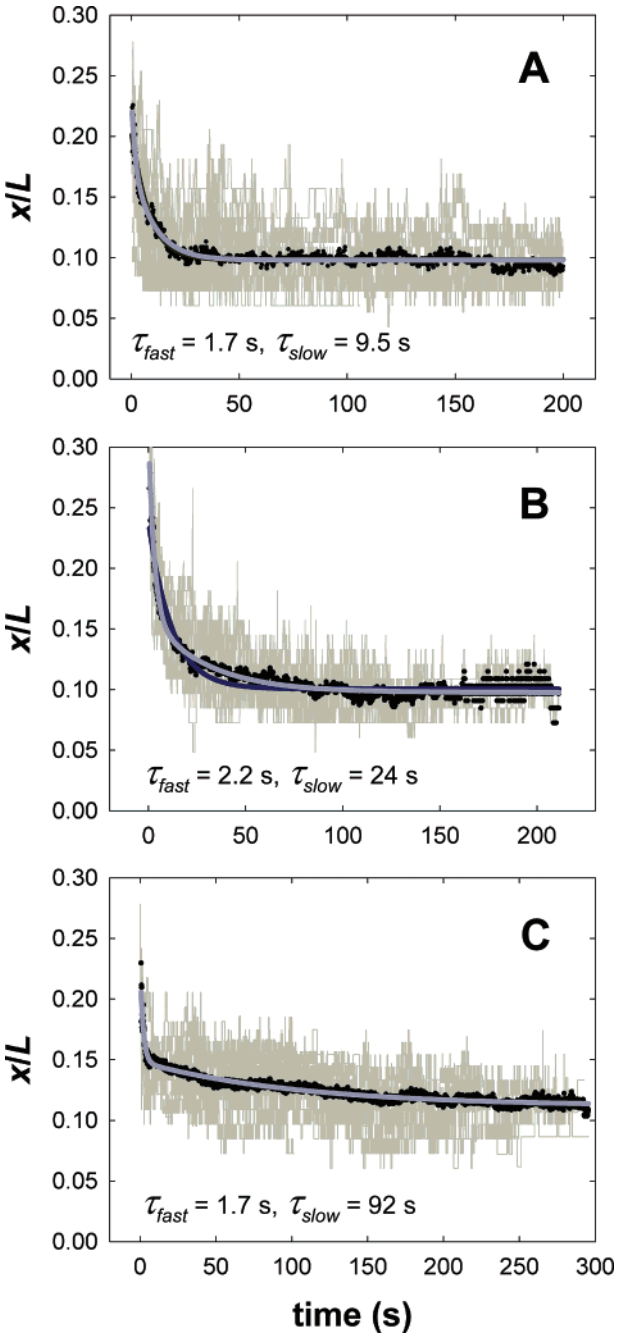

Figure 7. Single-molecule fractional extension relaxations (light-gray lines) at (A) 16 c^* ($N = 25$), (B) 23 c^* ($N = 19$), and (C) 35 c^* ($N = 23$) after ~13 strain at $\dot{\gamma} > 1000\ s^{-1}$. Black circles denote the average trajectory and gray lines represent double-exponential fits. For the two lower concentrations, a single-exponential fit (dark-gray line) is also shown for comparison in (A) and (B). The fits shown here were made to the unsquared extension for presentation purposes, whereas characteristic times were calculated for the squared quantity to maintain consistency with the methodology used in past single-molecule relaxation measurements.

govern retraction. To give a fair quantitative comparison, we estimated τ_R for stained λ-phage DNA at our solvent viscosity of 0.95 cP. Hur et al. studied the relaxation of dilute λ-phage DNA with Brownian dynamics simulations of a wormlike chain.[58] Using a method identical to the one used in single-molecule relaxation measurements,[24,26,27,39,59,60] he found that the relaxation times of simulated chains underpredicted the theoretical longest Rouse relaxation time by only 10%. Hence, we expect the present relaxations, also measured with an identical procedure, to have underestimated the longest Rouse by a similar amount. The Rouse time scale used in entangled theory, however, is not the longest Rouse but the rotational Rouse, which is identically a factor of 2 larger.[7,61] Hence, for our single-molecule measurement of dilute λ-phage DNA in a waterlike viscosity of 0.95 cP of $\tau = 0.089$ s (see Supporting Information), we should expect $\tau_R \approx (0.089)(1.0/0.9)(2) = 0.20$ s.

To verify this estimate, we employed the expression given by Chopra and Larson for the longest Rouse relaxation time.[62] When multiplied by 2, the expression gives the rotational Rouse time:

$$\tau_R = 2\tau_1 \approx \frac{N}{N-1}\frac{\langle R^2\rangle_0}{3\pi^2 D_G} \approx 0.19\ \text{s} \qquad (2)$$

The above value was obtained as follows. We assumed a large number of beads, $N > 10$, typically $N = 40$ for discretizing this size DNA into a bead-springs chain, setting the prefactor $N/(N-1) \approx 1$. Smith et al. measured the center-of-mass diffusivity, D_G, of isolated, stained λ-phage DNA coils from video microscopy.[38] We adopted his value for TOTO-1 stained DNA after the appropriate correction for a YOYO-1 stain persistence length: $D_{YOYO} = D_{TOTO}(1.35/1.75)^{-2/5}$. This gave $D_G = 0.52\ \mu m^2/s$ without the need to rescale for the solvent because, in both his and the present experiment, identical viscosities were used (0.95 cP). We estimated the ensemble-average end-to-end vector at $\langle R^2\rangle_o = N_K b^2 = 2.90\ \mu m^2$ using the stained Kuhn length of $b = 0.132\ \mu m$ and $N_K = 167$ Kuhn steps measured elsewhere.[63] Alternatively, the same quantity may be obtained from the equilibrium radius of gyration, R_G, with $\langle R^2\rangle_o = 6R_G^2$. R_G was measured both by direct visualization: 0.65 μm,[27] or indirectly from D_G by assuming a Zimm-like diffusivity: 0.73 μm.[38] In either case we obtain a value similar to the previous estimation: $2.54-3.20\ \mu m^2$. Taking the higher value, the rotational Rouse still is at most only 0.21 s. This result suggests that the measured τ_{fast} is in fact ≈ 10-fold larger than τ_R, the quantity commonly assumed by entangled molecular theories.

We speculate that the reason why the rotational Rouse assumption has recently resulted in capable theories with at least partial success in reproducing rheology data is simply because, rather than measuring τ_R in a theory-independent way and then using its value in the model, theoretical models were instead fitted to rheology data, typically linear viscoelasticity, using τ_R and other quantities such as the plateau modulus as fitting parameters. This semiempirical procedure reflected the unavailability of a technique capable of measuring the intrinsic fluid time scales directly, and the resulting ambiguities introduced in the analysis as a result have been recognized.[23,61] Interestingly, in a recent paper, different methodologies used to extract τ_R from rheology data using different sets of assumptions were shown to lead to as much as 1 order of magnitude difference in estimations from the same dataset.[64] In another recent work,[65] the rheology of high-molar-mass polystyrenes were measured on silica-treated cavities to eliminate interfacial slip during step shear flows. These authors found that the separability time of nonlinear step shear flows, λ_{k1}, was 5−10 times larger than the estimated τ_R. In fact, roughly one-half of all published rheology data has shown inconsistencies in τ_R but have so far been attributed to experimental artifacts such as slip, imperfect step strain history, or transducer compliance.[66]

An alternative interpretation to the inconsistencies in τ_R is to argue instead that the fundamental quantity underlying all tube physics is the local friction coefficient, ξ, which is typically a

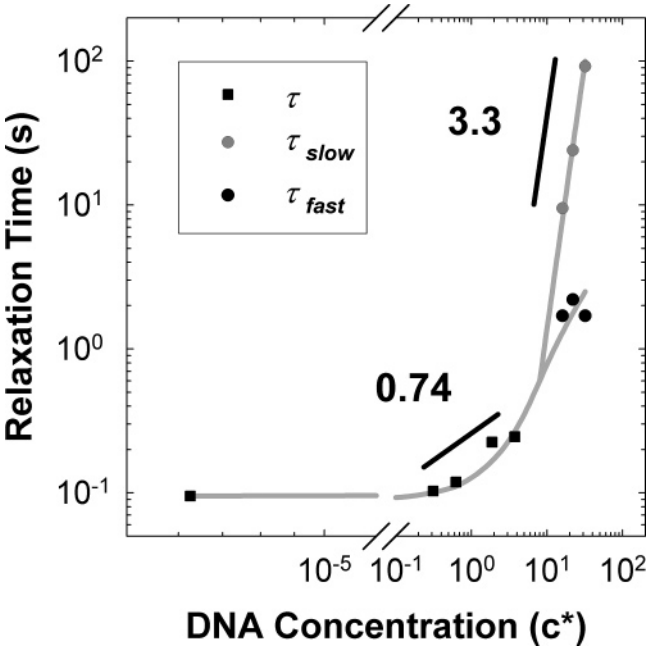

Figure 8. The relaxation times of λ-DNA spanning the dilute, semidilute, and entangled regimes in a solvent of 0.95 cP. Dilute and semidilute data are from Hur et al. The plot shows the power-law scalings during the semidilute transition to the entangled regime (0.74) and the entangled regime (3.3). It also shows a characteristic time splitting around 10 c^*.

priori unknown and must be fitted. Under this interpretation, the discrepancy remains the unusually large rise (in ξ) as concentration moves from dilute to entangled regimes.

What then is this larger tube retraction time scale (or, alternatively, the larger local friction coefficient)? At this point, we must recall that τ_R was initially chosen for simplicity. That is, as a first approximation, the chain retracts entropically along the tube at the same rate as it would in a dilute solution without being affected by the close proximity to other polymers undergoing the same process. Clearly, the actual retraction rate should have corrections. But can they account for an order of magnitude increase? Consider the case of DNA relaxing inside a long and narrow channel, much like a theoretical tube. Jendrejack et al. simulated such a case by taking into account hydrodynamic interactions between the polymer and channel walls of a square cross-section channel.[67] He found that the relaxation time doubled every time the channel width was decreased by a factor of 10 below a critical width of about 10 R_G. Other factors may also be important. For instance, the actual confinement space for any given chain is not a straight tube with a uniform cross-section but a contorted one, with regions of closer interactions between chain segments than others. The net effect may be the presence of frictional interactions between segments, which could slow down the retraction process beyond hydrodynamic interaction effects. Still, other nonidealities are likely to exist, including the possibility that the number of entanglements per chain may change during retraction. Exploring the effects of confinement on the retraction process with self-consistent computer simulations and novel microscopy techniques should prove useful in shedding light to this key issue.

Figure 8 shows our results together with dilute and semidilute λ-phage DNA data by Hur et al.[40] rescaled for our solvent viscosity and c^* estimation. In the dilute regime, the relaxation time remained nearly constant for over five decades in concentration. Approaching the semidilute regime, relaxation times ramped up, showing an approximate $\tau \propto c^{0.74}$ dependency during the transition. At around 10 c^*, a slower time scale split off from the faster chain retraction time scale. We tentatively assign this slower time scale to reptation because it was visually clear from our single-molecule observations that during this process chains searched for less oriented conformations via random center-of-mass displacements. This was in sharp contrast to the initial retraction, where chains merely shortened without reorienting or noticeably changing their positions. The reptation times appeared to converge to a straight line at high concentrations, giving a concentration dependency of $\tau_{slow} \propto c^{3.3}$, surprisingly close to the well-known molecular weight scaling of $M^{3.4}$. This was a considerably higher exponent than the disengagement time scaling predicted by reptation arguments,[48,56] $\tau_d \propto c^{1.5-3}$, or estimated from the zero-shear viscosity and elastic shear modulus,[55] $\tau_d \propto \eta_o/G_e \propto c^{2.7}$. Instead, it closely followed the characteristic separability time of the nonlinear step shear relaxation moduli:[55,65] $\lambda_{k2} \propto \tau_d \propto c^{3.2}$. From this, we must remain open to the possibility that reptation was not the only slow mechanism at work here and that CLF and constraint release (CR) could help explain the observed scaling[68] and are not inconsistent with our observations. In fact, CLF were easily noticeable in our observations as single chains stretched and retracted their ends at random orientations and time intervals (see movie in the Supporting Information). The concentration dependency of τ_{fast}, although not detectable in the present data, was likely much weaker than τ_{slow} but nonzero.

In what follows, we make two final but important observations regarding the relaxation measurements. In the average relaxation of the 35 c^* solution (Figure 7C), the transition between fast and slow decays became sharp enough to estimate the extension at the transition: $x/L \approx 0.15$. By definition, the primitive path length, L_{pp}, is the equilibrium curvilinear length of the tube, or the length a stretched entangled chain must shrink to before it is allowed to reorient. Hence, we regard this extension as L_{pp}, which for λ-phage DNA in a 35 c^* solution was $L_{pp} \approx 3.3$ μm. The primitive path length sets the dynamics of all entangled processes[23] and so is a key theoretical parameter of entangled solutions. Here, we have demonstrated a theory-independent and direct way to measure L_{pp} that should prove useful in future experiments. Later in this paper, our measure will be put to use in the comparison between single-molecule observations and the ROLIE-POLY model.

Finally, we point out the fact that single-molecule relaxation trajectories (light-gray lines) may have differed considerably between two identical chains, both starting from equilibrium and subjected to identical flow histories. Indeed, it was not uncommon to find, right after cessation of shearing and in the same image plane, one molecule significantly stretched ($x/L \approx 0.4$) and another one nearly completely coiled. For all three concentrations, the standard deviation of the distribution around each point in time was typically $\approx 30\%$ of the mean. This is evidence that molecular individualism was present in these experiments. In the next two sections, we will explore molecular individualism in more detail.

Steady Shear Flow

Entangled solutions were also studied under a constant applied shear flow. Steady-state data was taken after the initial transient evolution, lasting at most 130 s from equilibrium. In a fashion similar to the dilute case,[27,69] entangled polymers also underwent incessant stretch−collapse cycles (Figure 9). Here, we show examples of typical single-molecule extension (x) fluctuations over time at 35 c^*. Part A shows the zero shear flow case, where

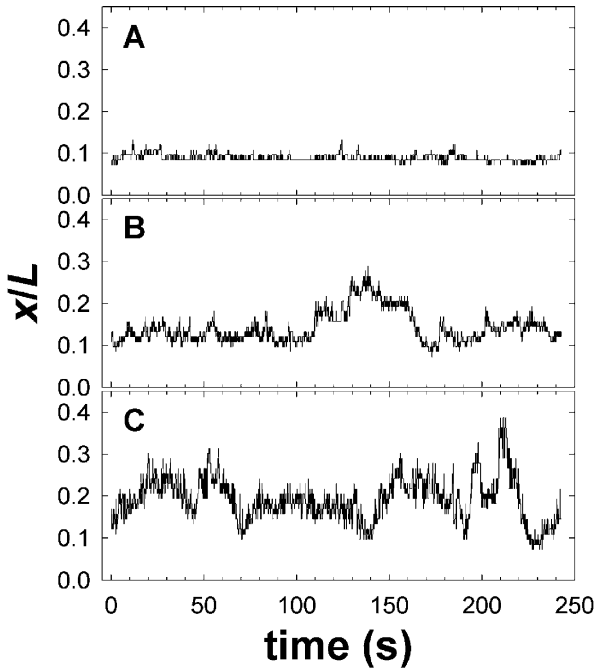

Figure 9. Fractional extension trajectories of single λ-DNA polymers in a 35 c^* solution. (A) At equilibrium in $\dot{\gamma} = 0$. (B and C) In an applied shear rate of $\dot{\gamma} = 1.3\ s^{-1}$ ($\dot{\gamma}\tau_{fast} = 2.6$) and $\dot{\gamma} = 2.7\ s^{-1}$ ($\dot{\gamma}\tau_{fast} = 5.4$), respectively.

the fluctuations of an equilibrated chain were driven solely by Brownian motion. In part B, the shear rate was $1.3\ s^{-1}$, giving $\dot{\gamma}\tau_{fast} = 2.6$ and $\dot{\gamma}\tau_{slow} = 120$ using the time scales measured from single-molecule relaxation. Periods of significant molecular extension are noticeable at $\dot{\gamma}\tau_{fast} = 2.6$, with fluctuations spanning the equilibrium baseline average of $\langle x\rangle/L \approx 0.096$ to ≈ 0.3. At $\dot{\gamma}\tau_{fast} = 5.4$ and $\dot{\gamma}\tau_{slow} = 248$ (C), the frequency, as well as the amplitude of stretch−collapse motions increased further, reaching ≈ 0.4. Notice that this same shear rate in the dilute regime would have imparted almost no deformation to the chain because, for that case, $\tau \approx 0.089$ s and $\dot{\gamma}\tau \approx 0.24 < 1$.

The pre-averaging approximation used in nearly all analytical molecular theories assumes that conformational distributions throughout the fluid are narrow. If instead they are broad, this approximation introduces errors proportional to the width and shape of the distribution. Current tube theoretical notions hold that large conformational changes and broad distributions may only be possible at $\dot{\gamma}\tau_R > 1$, deep inside the so-called tube-stretching regime.[23] To test this notion, we recast the observed fluctuations of several molecules as probability distributions for all concentrations and three shear rates (Figure 10). Our data shows that in all concentrations the distributions were broad for $\dot{\gamma}\tau_{fast} > 1$ and not $\dot{\gamma}\tau_R > 1$. For example, for $\dot{\gamma} = 0.3\ s^{-1}$ ($\dot{\gamma}\tau_{fast} = 0.6$), the lowest nonzero shear rate probed, the variance of the distribution was merely $\approx 0.14\ \mu m^2$. But for $\dot{\gamma} = 2.7\ s^{-1}$ ($\dot{\gamma}\tau_{fast} = 5.4$), the variance broadened dramatically to $\approx 2.2\ \mu m^2$. As we have shown that τ_{fast} is not τ_R but a value 1 order of magnitude higher, the tube-stretching regime was reached at much lower shear rates than expected. The semidilute, 10 c^* solution, also shows broad distributions. For this case, we used a time scale of $\tau \approx 1$ s estimated from the data in Figure 8.

Still, this evidence does not by itself disallow the pre-averaging approximation; for different molecules, even though they may deform extensively, they may do so in a concerted way, still giving a narrow distribution. Judging from individual trajectories in the extension relaxation experiments where

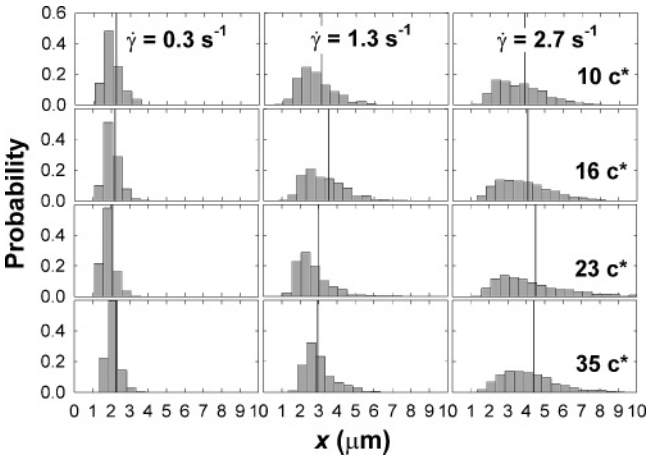

Figure 10. Extension probability distributions for three shear rates (columns) and four concentrations (rows). The sample size used in each distribution varied from $N = 2400$ to 7800. Vertical solid lines denote the mean of the distribution. Bins are 0.5 μm wide. In total, 492 molecules, 2.8×10^4 strains, and 3.6×10^5 images were recorded during all single-molecule experiments.

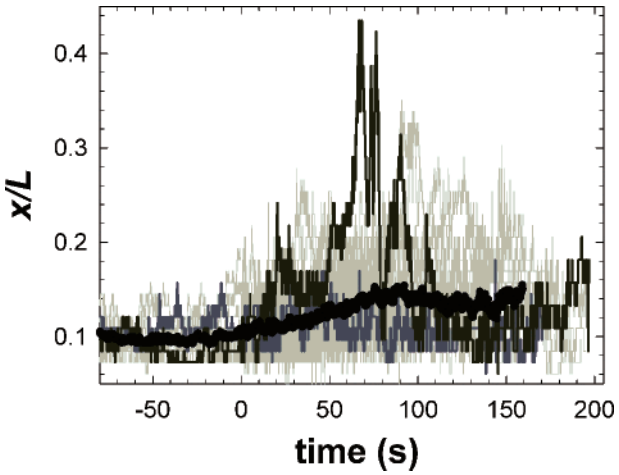

Figure 11. Transient response to the sudden inception ($t = 0$) of shear at $1.3\ s^{-1}$ ($\dot{\gamma}\tau_{fast} = 2.6$) and 35 c^*. The fractional extension trajectories of 30 individual molecules are shown (light-gray lines). Of those trajectories, two extreme cases, of large stretches (dark-gray line) and almost no stretch (gray line) are emphasized. Black circles represent the average trajectory. Before flow inception ($t < 0$), each molecule was at thermal equilibrium under no flow.

molecular individualism evolved from equilibrium, this does not seem to be the case. But to investigate this further, we looked at what happened to equilibrated molecules when subjected to a sudden shear flow.

Startup Shear Flow

The transient response was investigated at the single-molecule level for the highest concentration, 35 c^*. In the beginning, flow was stopped and molecules were allowed to equilibrate for a sufficiently long period of time, $t > 10\tau_{slow}$, as before. Then, a chain was chosen at random and molecular images were recorded. Some 50 s later, a sudden and constant shear flow of $1.3\ s^{-1}$ ($\dot{\gamma}\tau_{fast} = 2.6$) was applied and the molecule was followed for another 150−200 s. Figure 11 plots the individual fractional extension trajectories of 30 such molecules (light-gray lines). The large scatter in the trajectories relative to the baseline Brownian fluctuations at equilibrium ($t < 0$) is a clear indication of molecular individualism. To better illustrate this point, two extreme cases are emphasized in the plot. The dark-gray line shows a molecule that underwent a very rapid and dramatic

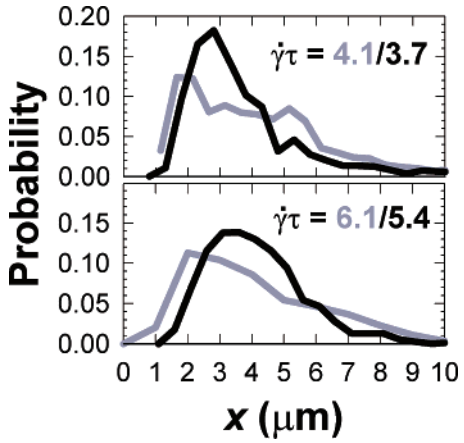

Figure 12. Extension distributions for 35 c^* entangled (black lines) and dilute solutions (gray lines). As before, for dilute fractional extensions, τ represents the longest polymer relaxation time, and for entangled solutions, $\tau = \tau_{fast} = 2.0$ s. Bins are 0.5 μm wide.

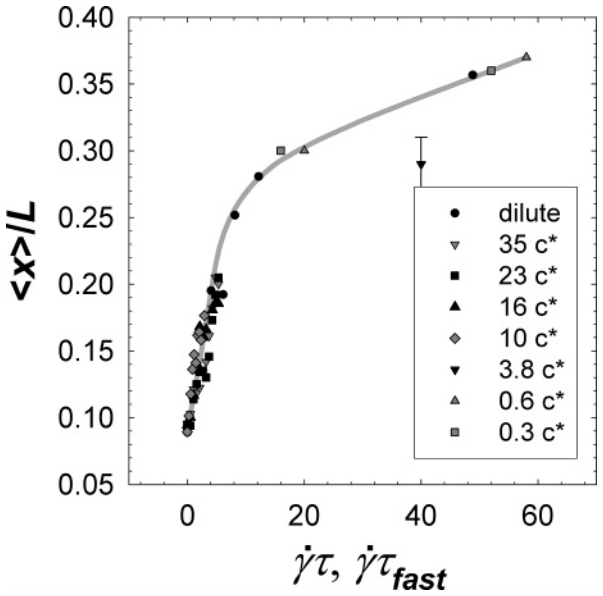

Figure 13. Mean fractional extensions of dilute, semidilute, and entangled solutions. Teixeira et al. and Hur et al. provided data for the dilute and semidilute regimes, respectively. For dilute fractional extensions, τ represents the longest polymer relaxation time, and for entangled solutions, $\tau = \tau_{fast} = 2.0$ s.

extension about 60 s after inception of flow. This extension took it momentarily past $x/L = 0.4$ and then was followed by two other rapid fluctuations, peaking successively at 0.3 and 0.2. In contrast, the other trajectory (gray line) suffered almost no extra deformation due to flow for the entire duration of the experiment.

Molecular individualism in various flow types was first observed in single-molecule experiments of dilute polymer solutions.[24−26,60,70] We speculate that, in entangled solutions, like dilute solutions, the particular orientations of the initial equilibrium conformations also play a role in later evolution. Unlike the dilute case, however, the relative orientations of neighboring chains should also have a direct influence, but because they were invisible, it is impossible to draw any predictions based on the initial state. Taken together, the existence of molecular individualism and the development of broad conformational distributions under $\dot{\gamma}\tau_{fast} > 1$ flows suggest a limit to the applicable shear rate range of the pre-averaging approximation and help to explain why molecular theories have repeatedly had difficulty in reproducing even bulk behavior under fast shear flows.

Entangled versus Dilute

The molecular extension distributions of entangled and dilute polymers are strikingly similar when shear rates are made dimensionless with τ_{fast} (measured earlier) for the entangled regime and the longest polymer relaxation time, τ, for the dilute regime (Figure 12). This correspondence is put into better perspective in Figure 13. In this figure, mean fractional extensions, $\langle x\rangle/L$, computed from steady shearing data, are shown for the four concentrations in the present experiments and a previously published experiment in a dilute solution.[27] The dilute dataset shown was chosen for simplicity of presentation, whereas a much larger volume of data exists from both single-molecule experimentation[26,27] (and Supporting Information) and Brownian dynamics simulations,[58,71] establishing the curve with a high precision. Extensions from all concentrated solutions show a clear overlap (within scatter), with the dilute curve for at least the initial rise in the case of entangled solutions, $\dot{\gamma}\tau_{fast} < 5.4$. Additionally, semidilute data from Hur et al.[40] for 0.3, 0.6, and 3.8 c^* λ-DNA also matches all other datasets, in this case, all the way to $\dot{\gamma}\tau = 60$.

This match among vastly different concentrations suggests that the collective effects of interacting neighboring chains under shear flow mimic simple dilute hydrodynamics, the effects of diffusion and flow advection coupled by the polymer backbone. In the semidilute regime, it was concluded that interacting chains operated as a mean-field enhancement of the (effective) solvent viscosity, resulting in longer characteristic polymer time scales relative to the dilute regime.[39,40] In the entangled regime, it shows that shear flows in the $\dot{\gamma}\tau_{fast} > 1$ range are dominated by the chain retraction time scale, τ_{fast}. This result is consistent with the formulation of the entangled chain undergoing essentially curvilinear Rouse dynamics inside the tube. The basic assumption here is that, while the source of forcing is different, a local drag arising from advecting topological constraints instead of a hydrodynamic drag, the outcome is still Rouse-like dynamics, with the only difference that the equilibrium length is now the primitive path length.[23] This observation does not contradict the previous finding that $\tau_{fast} \approx 10\tau_R$ from extension relaxations, it merely suggests that rather large corrections on τ_R are required while maintaining the Roussian form of the evolution equations. In other words, the tube not only produces deformation via topological constraints, but also modifies the unconstrained time scales within it.

The match with the dilute curve also suggests that, like the dilute case, a finitely extensible chain with a nonlinear elasticity may be required to capture the correct chain stretch under very fast shear flows, while a linear-spring Rouse chain would overpredict the stretch. In all recorded data, stretches of up to ≈ 8 μm, or $\langle x\rangle/L \approx 0.4$, were found often at the highest shear strength, $\dot{\gamma}\tau_{fast} = 5.4$ and $\dot{\gamma}\tau_{slow} = 248$. At this stretch, the force-extension curve of an isolated DNA has already departed somewhat from the linear force-extension response. Should this trend continue, the Rouse chain should become an increasingly poor modeling choice at $\dot{\gamma}\tau_{fast} > 1$. We also expect Rouse chains to introduce even larger errors in strong flow types (e.g., extensional flows), where the tendency to stretch is greater.

Comparison to the ROLIE-POLY Model

Our single polymer data represents a molecular-level benchmark for unambiguously evaluating molecular theories. In this section, we present one such evaluation. As this is the first analysis of this kind, we opted for the ROuse−CCR tube model

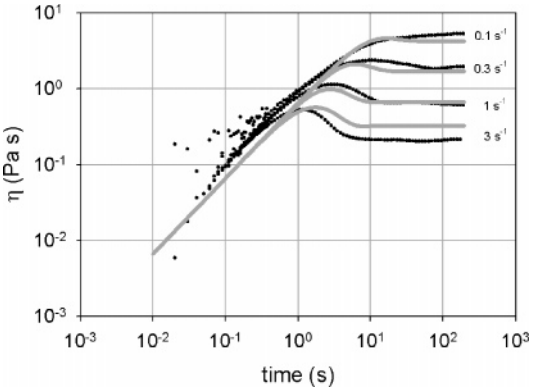

Figure 14. Comparison between the startup shear stress of a 23 c^* λ-DNA solution (black circles) to the ROLIE-POLY (gray lines) model. The RP model used the time scales obtained in the extension relaxation experiments: $\tau_{slow} = 24$ s and $\tau_{fast} = 2.2$ s. The vertical scale, G_e, was arbitrarily set to 1.5 Pa to facilitate presentation.

for LInear Entangled POLYmers, or RP for short (ROLIE-POLY) model of Likhtman and Graham[19,37] due to its relative simplicity, while still capturing, at least qualitatively, a broad range of viscoelastic features. The RP model is a simplified, single-mode version derived from the full multimode (contour variable) model proposed by the same authors elsewhere.[18] Even so, the RP version maintains the same comprehensive set of relaxation mechanisms and self-consistency closures from its multimode predecessor. This set of model ingredients has been proven indispensable to accurately capture rheological behaviors in both slow and fast flows simultaneously. These are reptation, convective- and reptation-driven constraint release, chain stretch, and contour length fluctuations. The RP equation has the final form:

$$\frac{d\sigma}{dt} = \kappa\cdot\sigma + \sigma\cdot\kappa^{T} - \frac{1}{\tau_d}(\sigma - \mathbf{I}) - \frac{2(1-\sqrt{(3/Tr\sigma)})}{\tau_R} \times \left(\sigma + \beta\left(\frac{Tr\sigma}{3}\right)^{\epsilon}(\sigma - \mathrm{I})\right) \quad (3)$$

where σ is the polymer stress tensor in units of the entanglement plateau modulus G_e. The velocity gradient tensor, κ, takes the form $\kappa = \dot{\gamma}\delta_{i2}\delta_{j1}$ in simple shear flow (δ is the Kronecker delta). The disengagement (reptation) and Rouse times are denoted by τ_d and τ_R, respectively. Tr denotes the trace, and $\mathbf{I} = \delta_{ij}$. The parameter β is the CCR coefficient analogous to c_v in the full theory. This CCR rate was defined as the average number of retraction events required to produce one tube hop of a tube diameter.[16] The authors have consistently used the value of $c_v = 0.1$ or, equivalently, $\beta = 1$, to describe experimental data. We use the same value here. The ad hoc exponent ϵ was set to -0.5 to give optimal results in their work. Again, we kept the same value for our analysis.

As a quick validation, we compared the RP model to our bulk rheology of λ-phage DNA. Figure 14 shows the startup shear response for 23 c^*. In such comparisons, G_e is usually treated as a tunable quantity, although in principle it can be predetermined from concentration and molecular parameters alone. Here, we have used $G_e = 0.8$ Pa to facilitate the presentation of results. The single-mode RP is able to reproduce the trends seen in the transient response but fails to achieve quantitative precision. The authors argue that, in the tube stretching regime, $\dot{\gamma}\tau_R > 1$, chains stretch sufficiently to justify the incorporation of nonlinear terms in the linear Rouse chain, thus correcting toward a finite extensibility.[37]

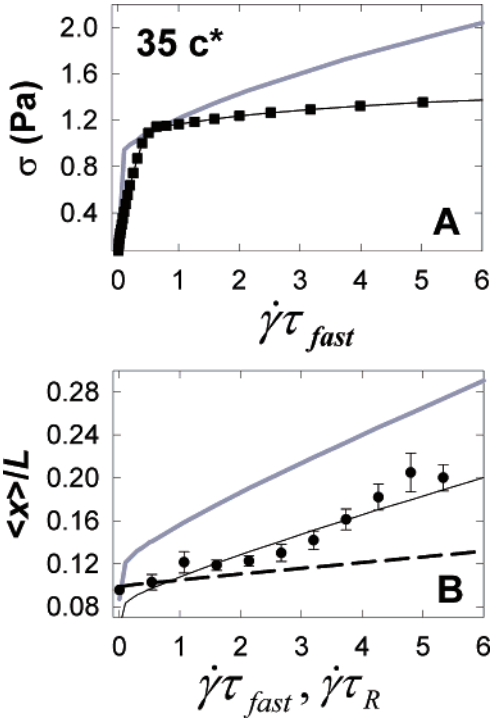

Figure 15. (A) Comparison between the shear stress of the 31 c^* solution under varying steady shear rates (black squares) and the RP model (gray line). Again, the vertical scale was set arbitrarily. (B) Mean fractional extensions from experiment (black circles), the RP model (gray line), and Brownian dynamics simulation by Neergaard and Schieber (dashed line). Here we used $L_{pp} \approx 3.3$ μm, measured directly from extension relaxations to set the length scale for the RP prediction. The thin black line represents the RP model with $L_{pp} \approx 2.3$ μm to give the best fit to experiment.

To test the predictive power of the RP equation against our single-molecule benchmark, we need to recast the information contained in the bulk stress tensor or, equivalently, the average molecular conformation, $\boldsymbol{\sigma}$, as mean fractional extensions, $\{\langle x\rangle/L$. The end-to-end stretch of the average RP chain is defined as $\lambda = \sqrt{Tr\boldsymbol{\sigma}/3}$ and in units of L_{pp}. Because our single-molecule measure is the maximum projected chain extension in the flow (or "1") direction, we take the projected stretch: $\lambda_{11} = \sqrt{\boldsymbol{\sigma}_{11}/3}$ and write:

$$\frac{\langle x\rangle_{RP}}{L} \approx \frac{L_{pp}}{L}\sqrt{\frac{\sigma_{11}}{3}} \quad (4)$$

This relationship is approximate because the molecular extension is not the end-to-end chain distance. Both quantities are identical only when the endpoints of the real chain are extended out along the flow direction, which is often the case. If the ends are folded, then the extension is greater than the end-to-end distance.

Equation 3 was time-stepped using a fourth-order Runge−Kutta numerical algorithm with $dt = \tau_R/10$. Our solutions showed convergence of at least six decimal places at this step size. In Figure 15, we show both bulk rheology (A) and single-molecule (B) comparisons between experiment and theory. In (B), we have included a second theoretical result, this one from a Brownian dynamics simulation by Neergaard and Schieber.[72] Their model consisted of $3\langle Z\rangle_{eq} = \tau_d/\tau_R = 3(7) = 21$ finitely extensible entropic springs in a constraining tube of Z segments. A self-consistent, mean-field CR mechanism was also added. They reported the "overall stretch ratio" as their microscopic observable. They defined it as "the ratio of the present average chain contour length to the average contour length of a chain

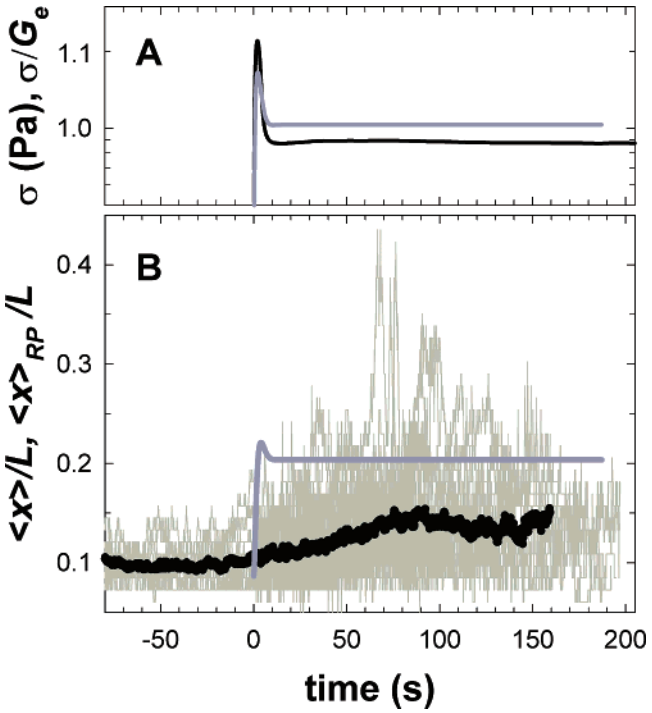

Figure 16. Testing the ROLIE-POLY model against experiment of both bulk and single-molecule responses to the startup of shear flow. The experiments were done on the samples with the highest concentration (31−35 c^*) and for shear rates between 1.0 and 1.3 s^{-1} ($\dot{\gamma}\tau_{fast} \sim 2.0-2.6$) (A) Shear stress curves for experiment (black line) and RP (gray line). The RP curve was made dimensionless with an arbitrary G_e scale to facilitate presentation. (B) Single-molecule fractional extension evolutions (also shown in Figure 11). Here, the average molecular extension trajectories are shown for experiment (black circles) and the RP model (gray line).

at equilibrium." Here, we translate this quantity as approximately the ratio $\langle x\rangle/\langle x\rangle_o$ and convert it to fractional extensions by multiplying $\langle x\rangle_o/L = 0.1$ to enable a comparison with our λ-phage DNA.

The RP model was able to capture the overall trend in both cases but obtained poor numerical agreement. For the single-molecule case, we used the equilibrium primitive path length obtained from relaxation experiments: $L_{pp} \approx 3.3\ \mu$m. With this value, the model overpredicted the mean fractional extensions by 40%. Alternatively, L_{pp} may be obtained via the definition: $L_{pp} = aZ$, or tube diameter, a, multiplied by the number of entanglements per chain, Z. These two quantities were obtained from Ferry's "temporary network" formula,[44] as before. From linear oscillatory shear data (Figure 6B, black triangles), we estimated $G_N^{(0)} \approx 2.7$ Pa, giving $Z = M/M_e \approx 22$, $a = b\sqrt{N_k/Z} \approx 0.4\ \mu$m, and $L_{pp} \approx 8.2\ \mu$m. This value, however, worsened the overprediction. The best fit to experimental data was found with $L_{pp} \approx 2.3\ \mu$m. Neergaard and Schieber's average "stretch ratio" was obtained from the full distribution of the ensemble. Nevertheless, their result underpredicted the experimental extensions. We do not expect that this discrepancy is due to differences in concentration because, as seen previously, fractional extension curves overlap when made dimensionless with τ_{fast} and L.

In Figure 16, we plot previous data on the transient response to a sudden shear rate (of 1.3 s^{-1}), together with RP model predictions for both bulk and single-molecule parameters. In our analogous bulk experiments (performed at 31c^* and at a shear rate of 1.0 s^{-1}), we observed a stress maximum appearing after only 2 s of shearing (A, black line), while at the molecular level, the mean fractional extension took much longer to develop (B, black circles), peaking slightly at around 90 s before reaching a steady level after $\approx$ 130 s. As in previously published dilute solution experiments, a peak in shear stress preceded a peak in extension.[39,40] In the dilute regime, this occurs due to the initial polymer stretch producing an increase in shear stress up to the point where the chain cannot stretch any further due to its finite extensibility. After this, the chain starts to align, thus reducing the shear stress. The molecular underpinnings for shear stress, namely the ensemble-average dimension of polymers in the shear gradient direction, was experimentally demonstrated elsewhere[27] but remains unverified for entangled polymers in the present study. In contrast to the dilute regime, the entangled case presents a much wider separation in strain between the stress and extension peaks.

The RP model correctly predicts the moment where the stress maximum appears (A, gray line), but its concomitant molecular extension also peaks early, displaying a behavior similar to the bulk and not the molecular scale (B, gray line). We point out that the discrepancies between theory and experiment cannot be attributed to our estimate of the end-to-end distance in molecular extension, as these errors are too small. We believe, rather, that the evidence illustrates a limitation in the model. To be fair, the authors of the RP model themselves have already stated that their equation is meant only as a simplified form amenable to calculations of complex flow geometries and should not be used to obtain molecular information. For that, full contour variable models should provide fairer comparisons and better tests for current physical notions. There are already cases in the literature showing that contour variable models are necessary to reproduce experiments probing beyond bulk rheology. Two noteworthy examples are the SANS structure factor predictions by the Graham−Likhtman−Milner−McLeish theory[19] and the extinction angle reproduction by the Mead−Larson−Doi theory.[15] Consequently, a good match with the single-mode version of the RP model should not have been expected. At this point, we pose the question of whether contour-variable models, with or without finitely extensible springs, are capable of reproducing single-molecule data. It is possible that the inherent limitations of these models due to the need to introduce pre-averaging approximations, especially in light of the demonstrated molecular individualism, will render the description of the correct molecular dynamics under fast flows amenable only to stochastic computer simulations or other approximations, which explicitly account for the broad molecular configuration distributions. We look forward to the answer to these questions in future studies.

Conclusions

We have presented the observations of single, entangled polymers in several shear flow experiments. We began by describing in detail the methodology used to prepare concentrated DNA solutions and the apparatus that enabled single-molecule visualizations during the application of controlled shear flows. To determine the level of entanglement of the four concentrations prepared for this study, a series of rheological measurements were performed. It was found that three of the four solutions were entangled: 16, 23, and 35 c^*, whereas the lowest one, 10 c^*, was semidilute. The rheology data was also later used as a benchmark for comparison to a molecular theory.

In our single-molecule experiments, a small fraction of stained λ-phage DNA chains were mixed with the unstained and entangled chains in solution. This way the stained, visible chains consisted of our "test" chains, while the neighboring unstained, invisible chains formed the confinements. Single-molecule

visualizations were first performed on the conformational relaxations following the cessation of a fast, essentially "instantaneous" shear flow. At 16 c^*, the ensemble-average relaxation appeared to follow a single-exponential decay. For the next-higher concentration, 23 c^*, two relaxation characteristic times became apparent. Then, for the highest concentration, 35 c^*, the relaxation times were well separated ($\tau_{slow}/\tau_{fast} = 54$). We found that$\tau_{fast}$, the chain retraction time scale, was 2.0 $\pm$ 0.5 s and insensitive to concentration. We estimated that this value was $\approx$ 10-fold higher than the rotational Rouse time assumed by numerous molecular theories to govern chain retraction. The slower time scale, τ_{slow}, grew faster with concentration ($\propto c^{3.3}$) than was predicted by pure reptation arguments.[48,56] We speculated that this higher exponent might be evidence of the influence of constraint release and contour length fluctuations on the reptative processes.

The trajectories of single molecules were followed in time not only during relaxation but also during the transient response to a sudden applied shear flow. In all cases, they displayed a highly individualistic behavior. That is, any two identical polymers both starting out at equilibrium and experiencing identical flow histories could later be found simultaneously at vastly different conformations. These varied from an isotropic coil to a stretched state (up to $x/L \approx 0.4$) at $\dot{\gamma}\tau_{fast} = 5.4$. The individualism of entangled chains with their broad conformational distributions has a direct bearing on molecular theories. Because all analytical theories assume a narrow conformational distribution to utilize the pre-averaged chain approximation, the breadth in this conformational distribution may render this approximation very poor. We speculate that the development of broad conformational distributions and molecular individualism under $\dot{\gamma}\tau_{fast} > 1$ flows limit the applicable shear rate range of the pre-averaging approximation and helps to explain why molecular theories have repeatedly had difficulty in reproducing even bulk behavior under fast shear flows.

We also showed that mean fractional extension data for entangled polymers overlapped with dilute and semidilute polymers when the shear rate was made dimensionless with τ_{fast}. This match among vastly different concentrations showed that shear flows in the $\dot{\gamma}\tau_{fast} > 1$ range were dominated by the chain retraction time scale, τ_{fast}, and corroborated the idea that entangled chains undergo essentially curvilinear Rouse dynamics inside the tube (but with a 10-fold higher characteristic time scale than the Rouse time). The favorable comparison with the dilute conformation data also suggests that, like the dilute case, a finitely extensible chain with a nonlinear elasticity may be required to capture the correct chain stretch under very fast shear flows, while a linear-spring Rouse chain would overpredict it. In future single-molecule studies, investigating very fast shear flows may reveal the importance of nonlinear force-extension functions; and a detailed look in the $\tau_{slow}^{-1} < \dot{\gamma} < \tau_{fast}^{-1}$ range will likely be of great value for investigating CCR ideas.

Last, we compared the ROLIE-POLY model[37] to fractional extensions under steady and transient shear flows. We showed that, under steady shear, the model captured the trends of both bulk and single-molecule data, but in general overpredicted the single-molecule extension curve. In the transient response to a sudden applied shear flow, the theory showed an early peak in shear stress agreeing with our rheology measurements, but the theoretical extension peak also occurred early instead of the much more gradual molecular extension. Further theoretical work will be necessary to determine whether the more sophisticated contour variable molecular theories are capable of simultaneously reproducing bulk and molecular behaviors.

From our observations, it was unclear whether the observed extension fluctuations were, at least in part, due to end-over-end tumbling, as was observed for the dilute case.[27,71,73] Because our shear apparatus was confined to visualizations in the "flow-vorticity" plane and was not capable of resolving the gradient direction, a direct observation of tumbling was not possible. However, there were a few indications of tumbling. In several instances, it was apparent that a stretch−collapse−stretch event was preceded by one of the ends moving slightly out of focus, signaling a drift in the gradient direction, while the rest of the chain remained sharply focused. In the dilute regime, the direct observation of the tumbling process led to a more complete understanding of the interplay between diffusion and advection on the polymer chain.[27] Uncovering the analogous process for the entangled regime could potentially have similar rewards and with the concomitant benefit of unveiling dynamics in the shear gradient dimension. Future studies should also include the visualization of single entangled chains in extensional flows, for instance, to test molecular individualism ideas under startup elongational flows akin to what was accomplished in dilute solutions.[25,60]

Additionally, the observation of single entangled polymers is not limited to linear architectures. Ring polymers, as well as Y-, H-, four-way, and other junctions have already been synthesized with DNA.[74,75] These structures are stable at room temperature and very flexible. After a junction is formed, one may ligate the desired length of DNA to the overhangs protruding from the junction points to create arms of varying lengths. This process may also be extended to create more complex topologies with multiple branching points including any combination of junction types. By using the same strategy of staining a small fraction against an unstained, invisible background, both equilibrium and nonequilibrium conformations can be studied as we have herein for linear chains. One may also opt for having different architectures of stained versus unstained chains, for instance, to investigate star polymers in a network of linear polymers. Comparing this data to theoretical ideas should reveal a host of important information about entangled branched polymers.

Acknowledgment. We thank Prof. D. E. Smith for his useful suggestions concerning sample preparation and single-molecule instrumentation and B. Cui for her help with confocal microscopy. We are especially grateful to the generous help of R. S. Graham concerning molecular theory and the comparison to the ROLIE-POLY model. We also thank W. T. Juan, as this work would not have been completed if it were not for the many illuminating late night discussions with him. Finally, this work was supported by a grant from the Materials Research Science and Engineering Center Program of the National Science Foundation (NSF) under DMR 9808677.

Supporting Information Available: Relaxation times of dilute λ-phage DNA; mixing; DNA integrity; flow-vorticity apparatus validation (PDF). Movies of λ-phage DNA diffusing in solution and being sheared (AVI). This material is available free of charge via the Internet at http://pubs.acs.org.

References and Notes

(1) Edwards, S. F. *Proc. Phys. Soc.* **1967**, *92*, 9.
(2) De Gennes, P. *J. Chem. Phys.* **1971**, *55*, 572.
(3) Doi, M.; Edwards, S. F. *J. Chem. Soc., Faraday Trans.* **1978**, *74*, 1789−1801.
(4) Doi, M.; Edwards, S. F. *J. Chem. Soc., Faraday Trans.* **1978**, *74*, 1802−1817.

(5) Doi, M.; Edwards, S. F. *J. Chem. Soc., Faraday Trans.* **1978**, *74*, 1818−1832.
(6) Doi, M.; Edwards, S. F. *J. Chem. Soc., Faraday Trans.* **1979**, *75*, 38−54.
(7) Doi, M.; Edwards, S. *The Theory of Polymer Dynamics*; Clarendon: Oxford, 1986.
(8) Marrucci, G.; Grizzuti, N. *Gazz. Chim. Ital.* **1988**, *118*, 179−185.
(9) Pearson, D.; Herbolzheimer, E.; Grizzuti, N.; Marrucci, G. *J. Polym. Sci., Part B: Polym. Phys.* **1991**, *29*, 1589−1597.
(10) Mead, D.; Leal, L. *Rheol. Acta* **1995**, *34*, 339−359.
(11) Marrucci, G. *J. Non-Newtonian Fluid Mech.* **1996**, *62*, 279−289.
(12) Ianniruberto, G.; Marrucci, G. *J. Non-Newtonian Fluid Mech.* **1996**, *65*, 241−246.
(13) Ianniruberto, G.; Marrucci, G. *J. Non-Newtonian Fluid Mech.* **2000**, *95*, 363−374.
(14) Ianniruberto, G.; Marrucci, G. *J. Rheol.* **2001**, *45*, 1305−1318.
(15) Mead, D.; Larson, R.; Doi, M. *Macromolecules* **1998**, *31*, 7895−7914.
(16) Milner, S.; McLeish, T.; Likhtman, A. *J. Rheol.* **2001**, *45*, 539−563.
(17) Likhtman, A.; McLeish, T. *Macromolecules* **2002**, *35*, 6332−6343.
(18) Graham, R. S.; Likhtman, A. E.; McLeish, T. C. B. *J. Rheol.* **2003**, *47*, 1171−1200.
(19) Bent, J.; Hutchings, L. R.; Richards, R. W.; Gough, T.; Spares, R.; Coates, P. D.; Grillo, I.; Harlen, O. G.; Read, D. J.; Graham, R. S.; Likhtman, A. E.; Groves, D. J.; Nicholson, T. M.; McLeish, T. C. B. *Science* **2003**, *301*, 1691−1695.
(20) Blanchard, A.; Graham, R. S.; Heinrich, M.; Pyckhout-Hintzen, W.; Richter, D.; Likhtman, A. E.; McLeish, T. C. B.; Read, D. J.; Straube, E.; Kohlbrecher, J. *Phys. Rev. Lett.* **2005**, *95*, 166001−166004.
(21) Wischnewski, A.; Monkenbusch, M.; Willner, L.; Richter, D.; Likhtman, A. E.; McLeish, T. C. B.; Farago, B. *Phys. Rev. Lett.* **2002**, *88*, 058301−058304.
(22) Graham, R. S. Personal communication.
(23) McLeish, T. *Adv. Phys.* **2002**, *51*, 1379−1527.
(24) Babcock, H.; Teixeira, R.; Hur, J.; Shaqfeh, E.; Chu, S. *Macromolecules* **2003**, *36*, 4544−4548.
(25) Perkins, T.; Smith, D.; Chu, S. *Science* **1997**, *276*, 2016−2021.
(26) Smith, D. E.; Babcock, H. P.; Chu, S. *Science* **1999**, *283*, 1724−1727.
(27) Teixeira, R.; Babcock, H.; Shaqfeh, E.; Chu, S. *Macromolecules* **2005**, *38*, 581.
(28) Muller, R.; Pesce, J. J.; Picot, C. *Macromolecules* **1993**, *26*, 4356−4362.
(29) Ylitalo, C. M.; Kornfield, J. A.; Fuller, G. G.; Pearson, D. S. *Macromolecules* **1991**, *24*, 749−758.
(30) Mead, D. W. In *Proceedings of the 12th International Congress on Rheology*; Ait-Kati, A., Dealy, J. M., James, D. F., Williams, M. C., Eds.; Canadian Rheology Group: Quebec City, 1996.
(31) Oberhauser, J. P.; Leal, L. G.; Mead, D. W. *J. Polym. Sci., Part B: Polym. Phys.* **1998**, *36*, 265−280.
(32) Yavich, D.; Mead, D.; Oberhauser, J.; Leal, L. *J. Rheol.* **1998**, *42*, 671−695.
(33) Islam, M. T.; Sanchez-Reyes, J.; Archer, L. A. *Rheol. Acta* **2003**, *42*, 191−198.
(34) Mhetar, V.; Archer, L. *J. Polym. Sci., Part B: Polym. Phys.* **2000**, *38*, 222−233.
(35) Smith, D.; Perkins, T.; Chu, S. *Phys. Rev. Lett.* **1995**, *75*, 4146−4149.
(36) Perkins, T.; Smith, D.; Chu, S. *Science* **1994**, *264*, 819−822.
(37) Likhtman, A. E.; Graham, R. S. *J. Non-Newtonian Fluid Mech.* **2003**, *114*, 1−12.
(38) Smith, D.; Perkins, T.; Chu, S. *Macromolecules* **1996**, *29*, 1372−1373.
(39) Babcock, H.; Smith, D.; Hur, J.; Shaqfeh, E.; Chu, S. *Phys. Rev. Lett.* **2000**, *85*, 2018−2021.
(40) Hur, J.; Shaqfeh, E.; Babcock, H.; Smith, D.; Chu, S. *J. Rheol.* **2001**, *45*, 421−450.
(41) Jary, D.; Sikorav, J. L.; Lairez, D. *Europhys. Lett.* **1999**, *46*, 251−255.
(42) Pearson, D. S. *Rubber Chem. Technol.* **1987**, *60*, 439−496.
(43) Mhetar, V.; Archer, L. *J. Polym. Sci., Part B: Polym. Phys.* **2000**, *38*, 222.
(44) Ferry, J. *Viscoelastic Properties of Polymers*, 3rd ed.; Wiley: New York, 1980.
(45) Menezes, E.; Graessley, W. *Rheol. Acta* **1980**, *19*, 38.
(46) Bercea, M.; Peiti, C.; Simionescu, B.; Navard, P. *Macromolecules* **1993**, *26*, 7095−7096.
(47) Islam, M. T.; Archer, L. A. *J. Polym. Sci., Part B: Polym. Phys.* **2001**, *39*, 2275−2289.
(48) De Gennes, P. *Scaling Concepts in Polymer Physics*; Cornell University Press: Ithaca, NY, 1979.
(49) De Gennes, P. G.; Leger, L. *Annu. Rev. Phys. Chem.* **1982**, *33*, 49−61.
(50) Menezes, E. V.; Graessley, W. W. *J. Polym. Sci., Polym. Phys. Ed.* **1982**, *20*, 1817−1833.
(51) Attane, P.; Pierrard, J. M.; Turrel, G. *J. Non-Newtonian Fluid Mech.* **1985**, *18*, 295−317.
(52) Sanchez-Reyes, J.; Archer, L. A. *J. Rheol.* **2003**, *47*, 469−482.
(53) Osaki, K.; Inoue, T.; Isomura, T. *J. Polym. Sci., Part B: Polym. Phys.* **2000**, *38*, 1917−1925.
(54) Lodge, T. P.; Rotstein, N. A.; Prager, S. *Adv. Chem. Phys.* **1990**, *79*, 1−132.
(55) Sanchez-Reyes, J.; Archer, L. *Macromolecules* **2002**, *35*, 5194−5202.
(56) Schweizer, K. S.; Szamel, G. *Macromolecules* **1995**, *28*, 7543−7548.
(57) Press, W. H.; Teukolsky, S. A.; Vetterling, W. T.; Flannery, B. P.; Cambridge University Press: Cambridge, 1998; p 549.
(58) Hur, J.; Shaqfeh, E.; Larson, R. *J. Rheol.* **2000**, *44*, 713−742.
(59) Perkins, T.; Smith, D.; Chu, S. *Flexible Polymer Chains in Elongational Flow*; Springer: Berlin, 1999.
(60) Smith, D.; Chu, S. *Science* **1998**, *281*, 1335−1340.
(61) Larson, R.; Sridhar, T.; Leal, L.; McKinley, G.; Likhtman, A.; McLeish, T. *J. Rheol.* **2003**, *43*, 809.
(62) Chopra, M.; Larson, R. *J. Rheol.* **2002**, *46*, 831−862.
(63) Quake, S.; Babcock, H.; Chu, S. *Nature* **1997**, *388*, 151−154.
(64) Roland, C.; Archer, L.; Mott, P.; Sanchez-Reyes, J. *J. Rheol.* **2004**, *48*, 395.
(65) Archer, L.; Sanchez-Reyes, J.; Juliani. *Macromolecules* **2002**, *35*, 10216−10224.
(66) Venerus, D. *J. Rheol.* **2005**, *49*, 277−295.
(67) Jendrejack, R. M.; Dimalanta, E. T.; Schwartz, D. C.; Graham, M. D.; de Pablo, J. J. *Phys. Rev. Lett.* **2003**, *91*, 038102−038104.
(68) Rubinstein, M. *Phys. Rev. Lett.* **1987**, *59*, 1946.
(69) Smith, D.; Babcock, H.; Chu, S. *Science* **1999**, *283*, 1724−1727.
(70) De Gennes, P. *Science* **1997**, *276*, 1999.
(71) Schroeder, C.; Teixeira, R.; Shaqfeh, E.; Chu, S. *Macromolecules* **2004**, *38*, 1967−1978.
(72) Neergaard, J.; Schieber, J. *J. Non-Newtonian Fluid Mech.* **2002**, *105*, 111−130.
(73) Teixeira, R.; Schroeder, C.; Shaqfeh, E.; Chu, S. *Phys. Rev. Lett.* **2005**, *95*, 018301−018304.
(74) Seeman, N. C. *Annu. Rev. Biophys. Biomol. Struct.* **1998**, *27*, 225−248.
(75) Seeman, N. C. *Biochemistry* **2003**, *42*, 7259−7269.
(76) Milner, S. T.; McLeish, T. C. B. *Phys. Rev. Lett.* **1998**, *81*, 725.
(77) Larson, R. *The Structure and Rheology of Complex Fluid*, New York: Oxford, 1999.
(78) Xu, F.; Denn, M. M.; Schieber, J. D. *J. Rheol.* **2006**, *50*, 477−494.

MA062932E